Laser Speckle and Related Phenomena

Editor: J. C. Dainty

Second Enlarged Edition

7. Stellar Speckle Interferometry

J. C. DAINTY

With 19 Figures

The use of optical interferometry to determine the spatial structure of astronomical objects was first suggested by FIZEAU in 1868 [7.1]. Stellar interferometers measure, in modern terminology, the spatial coherence of light incident upon the Earth, and the object intensity (or some parameter such as its diameter) is calculated using the van Cittert–Zernike theorem [7.2]. FIZEAU's suggestion led to the development of specialized long baseline interferometers; MICHELSON's stellar interferometer [7.3, 4] directly applied Fizeau's method (amplitude interferometry), whilst the intensity interferometer of HANBURY BROWN and TWISS [7.5] enabled the squared modulus of the spatial coherence function to be measured for thermal sources.

Until recently, single optical telescopes were used in a conventional (non-interferometric) way, their spatial resolution being limited to approximately 1".0* due to the presence of atmospheric turbulence or "seeing". In 1970, LABEYRIE invented the technique of stellar speckle interferometry [7.6], in which diffraction-limited resolution is obtained from a large single telescope despite the seeing. The diffraction-limited angular resolution $\Delta\alpha$ of a telescope of diameter D operating at wavelength λ is conveniently expressed by the Rayleigh criterion,

$$\Delta\alpha = 1.22\frac{\lambda}{D}, \tag{7.1}$$

yielding approximately 0".025 at $\lambda = 400$ nm for a 4 m telescope. The first results by LABEYRIE and collaborators were published in 1972 [7.7] and since then approximately 250 papers on speckle interferometry have been published [7.8].

Labeyrie's important contribution was to recognize that the speckles formed at the focus of a large telescope have an angular size determined by diffraction, i.e. their smallest dimension is given by (7.1). Diffraction-limited information about an astronomical object can therefore be extracted from short-exposure, narrow-band images by an appropriate method of data reduction.

* One arc second.

This chapter is divided into six sections. The basic principles are outlined in non-mathematical terms in Sect. 7.1, and this is followed by a detailed mathematical discussion of the technique in Sect. 7.2. In astronomy, the objects under observation are often faint and only a limited observing time is available, so that the question of signal-to-noise ratio is very important; this is evaluated in Sect. 7.3. In Sect. 7.4 we discuss the problem of finding images (or maps) of astronomical objects using speckle data. This is an area of considerable activity at the moment both by theoreticians and observers. The equipment required to implement speckle interferometry is described in Sect. 7.5; this section includes a discussion of the technique of one-dimensional infra-red speckle interferometry which has proved so fruitful in recent years. Finally, we conclude with a brief summary of the astronomical results produced by speckle interferometry—these range from measurements of asteroids to quasars.

Certain topics have been deliberately omitted or are considered only very briefly. Other methods of interferometry, such as rotation-shearing interferometry [7.9] and long baseline interferometry [7.10, 15], are not considered. The discussion in Sect. 7.4 of the phase problem is incomplete due partly to the uncertainty in the field at the moment; a more complete exposition of this subject may be found in the review paper by BATES [7.11] which is complementary in content to this chapter. Earlier reviews of stellar interferometry may be found in [7.12–15]; some useful references are also contained in two conference proceedings [7.16, 17].

7.1 Basic Principles

Figure 7.1 shows highly magnified images of an unresolvable ("point") and a resolved star taken using a large telescope with an exposure time of approximately 10^{-2} s through a filter of bandwidth 10 nm. In the case of the point source (upper row), the image has a speckle-like structure and it is found that, as with conventional laser speckle patterns, the minimum speckle "size" is of the same order of magnitude as the Airy disc of the telescope. A long-exposure image is simply the sum of many short-exposure ones, each with a speckle structure that is different in detail, and is therefore a smooth intensity distribution whose diameter is typically 1″.0 in good seeing. Long-exposure images of the point source and resolved star of Fig. 7.1 would show little, if any, difference. The minimum speckle size, on the other hand, is approximately 0″.025 for a 4 m telescope at a mean wavelength of 400 nm; by extracting correctly the information in short-exposure images, it is possible to observe detail as

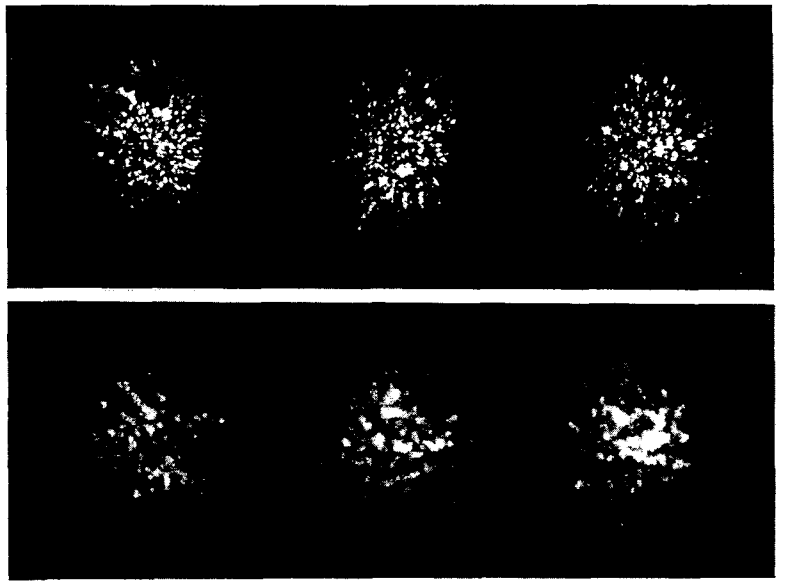

Fig. 7.1. Short exposure photographs of an unresolved point source (*upper row*) and a resolved star, α-Orionis, (*lower row*) taken on a 4 m-class telescope. The exposure time and filter bandwidth are 10^{-2} s and 10 nm, respectively (courtesy of B. L. Morgan and R. J. Scaddan, Imperial College, London)

small as the limit imposed by diffraction and not be limited to the 1″.0 resolution of conventional images.

A laboratory simulation illustrating the basic method is shown in Fig. 7.2 for an unresolved star, binary stars of two separations, and a resolved star (shown as a uniformly illuminated disc). A large number of short-exposure records are taken, each through a different realization of the atmosphere, typical examples being shown in row B. For a binary star, each component produces an *identical* speckle pattern (assuming isoplanatism and neglecting photon noise) and a "double-speckle" effect may be visible in each short-exposure image in favourable circumstances. The optical diffraction pattern, or squared modulus of the Fourier transform, of a typical short-exposure record is shown in row C for each object. The signal-to-noise ratio is low for a single record and may be improved by adding many such diffraction patterns (row D). The unresolved object has a diffraction halo of relatively large spatial extent, the binaries give fringes of a period inversely proportional to their separation, and the resolved object gives a diffraction halo whose diameter is inversely proportional to the diameter of the object. By taking a further

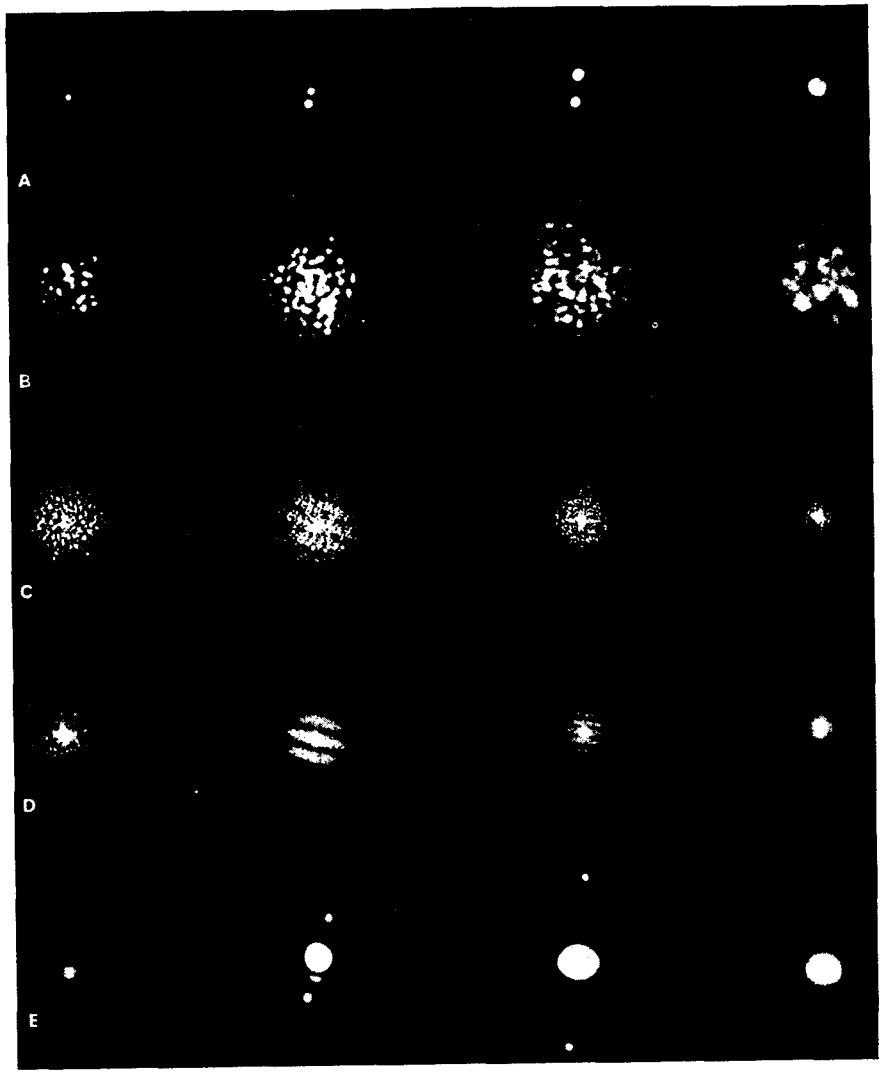

Fig. 7.2A–E. Laboratory simulation showing the principles of stellar speckle interferometry. (A: objects; B: typical short exposure photographs; C: diffraction patterns of row B; D: sum of 20 diffraction patterns; E: diffraction pattern of row D) (courtesy of A. Labeyrie, CERGA)

Fourier transform of each ensemble-average diffraction pattern we obtain the average spatial (or angular) autocorrelation of the diffraction-limited images of each object (row E).

The term "speckle interferometry" was adopted by GEZARI et al. [7.7]. The interferometer is, in fact, the telescope—light from all parts of the pupil propagates to the image plane where it interferes to become a speckle pattern. In other forms of stellar interferometry, the light in the pupil is combined in a different way, for example, using a rotation-shearing interferometer. The beauty of the speckle technique is that the interferometer (i.e., the telescope) is already constructed to the required tolerances.

7.2 The Theory of Speckle Interferometry

7.2.1 Outline of Theory

For each short-exposure record, the usual quasi-monochromatic, isoplanatic imaging equation applies, provided that the angular extent of the object is not too large[1]:

$$I(\alpha,\beta)=\int_{-\infty}^{\infty}\int O(\alpha',\beta')P(\alpha-\alpha',\beta-\beta')d\alpha'd\beta'$$

or, in notation,

$$I(\alpha,\beta)=O(\alpha,\beta)\circledast P(\alpha,\beta)\,, \tag{7.2}$$

where $I(\alpha,\beta)$ is the instantaneous image intensity as a function of angle (α,β), $O(\alpha,\beta)$ is the object intensity, $P(\alpha,\beta)$ is the instantaneous point spread function of the atmosphere/telescope system normalized to unit volume, and $\circledast$ denotes the convolution integral.

As we demonstrated in Sect. 7.1, the analysis of this data may be carried out in two equivalent ways. In the angular, or spatial, domain, the ensemble averaged angular autocorrelation function of the image is found; this is defined as

$$C_I(\alpha,\beta)\equiv\left\langle\int_{-\infty}^{\infty}\int I(\alpha',\beta')I(\alpha'+\alpha,\beta'+\beta)d\alpha'd\beta'\right\rangle,$$

or, in notation,

$$C_I(\alpha,\beta)\equiv\langle I(\alpha,\beta)*I(\alpha,\beta)\rangle\,, \tag{7.3}$$

[1] Throughout this review, the object and image plane coordinates are taken to be angles (α,β), the coordinates in the Fourier transform plane being angular frequencies (arc sec^{-1}).

where $*$ denotes angular autocorrelation. Combining (7.2 and 3) yields the following relationship between object and image autocorrelation functions,

$$C_I(\alpha,\beta)=C_O(\alpha,\beta)\circledast\langle P(\alpha,\beta)*P(\alpha,\beta)\rangle, \tag{7.4}$$

where $C_O(\alpha,\beta)$ is the angular autocorrelation function of the object intensity. Note that (7.4) for the object and image autocorrelation functions is similar in form to (7.2) for object and image intensities, but with an impulse response equal to $\langle P(\alpha,\beta)*P(\alpha,\beta)\rangle$.

In the angular (or spatial) frequency domain, the average squared modulus of the Fourier transform of the image intensity is found: this is correctly referred to as the average energy spectrum,[2]

$$\Phi_I(u,v)\equiv\langle|i(u,v)|^2\rangle, \tag{7.5}$$

where

$$i(u,v)\equiv\int_{-\infty}^{\infty}\int I(\alpha,\beta)\exp[-2\pi i(u\alpha+v\beta)]d\alpha\,d\beta. \tag{7.6}$$

Combining (7.2, 5 and 6) yields the following simple relationship between the energy spectrum of the image $\Phi_I(u,v)$ and that of the object $\Phi_O(u,v)$:

$$\Phi_I(u,v)=\Phi_O(u,v)\cdot\mathscr{T}(u,v), \tag{7.7}$$

where

$$\mathscr{T}(u,v)\equiv\langle|T(u,v)|^2\rangle,$$

and $T(u,v)$, the instantaneous transfer function, is equal to the Fourier transform of the point spread function,

$$T(u,v)=\int_{-\infty}^{\infty}\int P(\alpha,\beta)\exp[-2\pi i(u\alpha+v\beta)]d\alpha\,d\beta. \tag{7.8}$$

Because of the similarity between (7.7) and the Fourier-space isoplanatic imaging equation (in which image frequency components are equal to object frequency components multiplied by an optical transfer function [7.19]), the quantity $\mathscr{T}(u,v)$ is referred to as the transfer function for speckle interferometry or *speckle transfer function*. Equations (7.4 and 7) in the real (angular) and Fourier (angular frequency) domains respectively are completely equivalent; (7.7) is simply obtained by taking the Fourier transform of both sides of (7.4).

[2] The *energy spectrum* of a function equals the squared modulus of its Fourier transform. If the function is a realization of a square-integrable non-stationary random process, an *ensemble-averaged energy spectrum* can be defined as in (7.5). A realization of a stationary random process does not possess a Fourier transform, but a *power spectrum* can be defined in terms of a generalized Fourier transform [7.18].

The conventional ("long-exposure") image intensity is found from (7.2) by ensemble averaging:

$$\langle I(\alpha,\beta)\rangle=O(\alpha,\beta)\circledast\langle P(\alpha,\beta)\rangle, \tag{7.9}$$

where $\langle P(\alpha,\beta)\rangle$ is the average point spread function of the atmosphere/telescope system. In Fourier space, (7.9) becomes

$$\langle i(u,v)\rangle=o(u,v)\langle T(u,v)\rangle, \tag{7.10}$$

where $o(u,v)$ is the Fourier transform of the object intensity, and $\langle T(u,v)\rangle$ is the average, or long-exposure, transfer function.

Comparing conventional long-exposure imaging, (7.10), to speckle interferometry, (7.7), it is clear that the resolution of conventional imaging is governed by the form of the average transfer function $\langle T(u,v)\rangle$, whereas in speckle interferometry the relevant transfer function is $\mathscr{T}(u,v)\equiv\langle|T(u,v)|^2\rangle$. In the following sections we shall show that the latter function retains high angular-frequency information that is lost in conventional imaging. However, it must be remembered that $\mathscr{T}(u,v)$ is a transfer function for energy spectra, whereas $\langle T(u,v)\rangle$ is a transfer function for Fourier components; the loss of Fourier phase information in speckle interferometry is a severe limitation to its usefulness and possible methods of retrieving the Fourier phase will be discussed in Sect. 7.4.

7.2.2 The Long-Exposure Transfer Function

To find the optical transfer function of a system, we must consider the imaging of a quasi-monochromatic point source as in Fig. 7.3. For an isoplanatic, incoherent imaging system, the optical transfer function $T(u,v)$ is equal to the normalized spatial autocorrelation of the pupil function $H(\xi,\eta)$,

$$T(u,v)=\frac{\int_{-\infty}^{\infty}H(\xi,\eta)H^*(\xi+\lambda u,\eta+\lambda v)d\xi\,d\eta}{\int_{-\infty}^{\infty}\int|H(\xi,\eta)|^2d\xi\,d\eta}, \tag{7.11}$$

where (u,v) are angular frequency coordinates, (ξ,η) are distance coordinates in the pupil and λ is the mean wavelength [7.20]. The pupil function $H(\xi,\eta)$ is the complex amplitude in the exit pupil, relative to a reference sphere centered on the Gaussian focus, due to a point source

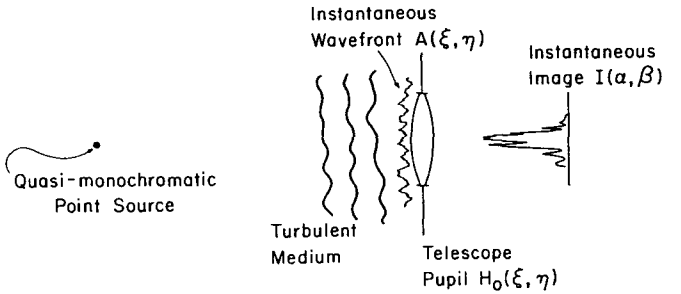

Fig. 7.3. The formation of an instantaneous image of a point source through the atmosphere

and in the case of propagation through the turbulent atmosphere may be written as

$$H(\xi,\eta)=A(\xi,\eta)H_0(\xi,\eta), \tag{7.12}$$

where $A(\xi,\eta)$ is the complex amplitude of light from a point source that has propagated through the atmosphere and $H_0(\xi,\eta)$ is the pupil function of the optical system alone.

Substitution of (7.12) into (7.11) gives

$$T(u,v)=\frac{\int\int_{-\infty}^{\infty} A(\xi,\eta)A^*(\xi+\lambda u,\eta+\lambda v)H_0(\xi,\eta)H_0^*(\xi+\lambda u,\eta+\lambda v)d\xi\,d\eta}{\int\int_{-\infty}^{\infty}|A(\xi,\eta)|^2\,|H_0(\xi,\eta)|^2 d\xi\,d\eta}. \tag{7.13}$$

The long-exposure or average transfer function is found by averaging (7.13). The lower line is simply the intensity of light integrated over the telescope pupil and is effectively constant for a large telescope and/or weak scintillation. We also assume that $A(\xi,\eta)$ is a (wide-sense) stationary process [i.e., its mean and autocorrelation function in (7.13) are independent of the ξ,η coordinates], so that the expression for the long-exposure transfer function becomes [7.21]

$$\langle T(u,v)\rangle = T_s(u,v)T_0(u,v), \tag{7.14}$$

where $T_s(u,v)$ is the atmospheric or "seeing" transfer function,

$$T_s(u,v)=\frac{\langle A(\xi,\eta)A^*(\xi+\lambda u,\eta+\lambda v)\rangle}{\langle|A(\xi,\eta)|^2\rangle}, \tag{7.15}$$

and $T_0(u,v)$ is the optical transfer function of the telescope alone,

$$T_0(u,v)=\frac{\int\int_{-\infty}^{\infty} H_0(\xi,\eta)H_0^*(\xi+\lambda u,\eta+\lambda v)d\xi\,d\eta}{\left\langle\int\int_{-\infty}^{\infty}|H_0(\xi,\eta)|^2 d\xi\,d\eta\right\rangle}. \tag{7.16}$$

Thus the long-exposure transfer function is equal to the product of the transfer functions of the atmosphere and telescope.

A detailed discussion of the atmospheric transfer function and other relevant properties of turbulence may be found in [7.22–25], particularly in the comprehensive review by RODDIER [7.24]. For a Kolmogorov spectrum of turbulence, the average transfer function is rotationally symmetric and is given by

$$T_s(w)=\exp\left[-3.44\left(\frac{\lambda|w|}{r_0}\right)^{5/3}\right], \tag{7.17}$$

where $w=\sqrt{u^2+v^2}$ and the parameter r_0, first defined by FRIED [7.22], is equal to the diameter of the diffraction-limited telescope whose Airy disc has the same area as the seeing disc. The parameter r_0 plays an important role in both long-exposure imaging and speckle interferometry; it can be shown that [7.24]

$$r_0 \propto \lambda^{6/5}(\cos\gamma)^{3/5}, \tag{7.18}$$

where γ is the zenith angle. Typical values of r_0 lie in the range 5 to 20 cm at a good observing site in the visible range; since an r_0 value of 10 cm at $\lambda=500$ nm is equivalent to $r_0=3.6$ m at $\lambda=10\,\mu$m, it follows that a 4 m class telescope is severely seeing-limited in the visible but essentially diffraction-limited at 10 μm.

The angular "diameter" of the seeing disc, or seeing angle ω, is defined by

$$\omega\equiv\frac{\lambda}{r_0}, \tag{7.19}$$

and is therefore proportional to $\lambda^{-1/5}$. At $\lambda=500$ nm and $r_0=10$ cm, the seeing disc has a diameter of approximately 5×10^{-6} rad or 1″.0.

Measurements of the long-exposure transfer function and the parameter r_0 have been reported by DAINTY and SCADDAN [7.26], RODDIER [7.27], and BROWN and SCADDAN [7.28] and there is good agreement with (7.17).

7.2.3 The Speckle Transfer Function

The transfer function of speckle interferometry, $\mathscr{T}(u,v) \equiv \langle |T(u,v)|^2 \rangle$, relates the average energy spectrum of the image to that of the object. Using (7.13), we can write $|T(u,v)|^2$ as $|T(u,v)|^2 = \mathscr{A}(u,v)/\mathscr{B}$, where

$$\mathscr{A}(u,v) = \int\int_{-\infty}^{\infty}\int\int A(\xi_1,\eta_1)A^*(\xi_1+\lambda u,\eta_1+\lambda v)A^*(\xi_2,\eta_2)$$
$$\cdot A(\xi_2+\lambda u,\eta_2+\lambda v)H_0(\xi_1,\eta_1)H_0^*(\xi_1+\lambda u,\eta_1+\lambda v)$$
$$\cdot H_0^*(\xi_2,\eta_2)H_0(\xi_2+\lambda u,\eta_2+\lambda v)d\xi_1 d\eta_1 d\xi_2 d\eta_2$$

and

$$\mathscr{B} = \left[\int\int_{-\infty}^{\infty} |A(\xi,\eta)|^2 |H_0(\xi,\eta)|^2 d\xi\, d\eta\right]^2 . \tag{7.20}$$

As before, $A(\xi,\eta)$ is assumed to be a stationary random process with weak scintillation; for convenience we define $\langle |A|^2 \rangle \equiv 1$ and the pupil area $\mathscr{S}$,

$$\mathscr{S} \equiv \int\int_{-\infty}^{\infty} |H_0(\xi,\eta)|^2 d\xi\, d\eta \tag{7.21}$$

(this is the true pupil area for an unapodized, or clear, pupil).

With the substitution $\xi' = \xi_2 - \xi_1$ and $\eta' = \eta_2 - \eta_1$, (7.20) yields the following expression for the speckle transfer function:

$$\mathscr{T}(u,v) = \mathscr{S}^{-2} \int\int_{-\infty}^{\infty} \mathscr{M}(u,v;\xi',\eta')\mathscr{H}(u,v;\xi',\eta')d\xi' d\eta' ,$$

where $\mathscr{M}$ is a fourth-order moment,

$$\mathscr{M}(u,v;\xi',\eta') \equiv \langle A(\xi_1,\eta_1)A^*(\xi_1+\lambda u,\eta_1+\lambda v)A^*(\xi_1+\xi',\eta_1+\eta')$$
$$\cdot A(\xi_1+\xi'+\lambda u,\eta_1+\eta'+\lambda v)\rangle \tag{7.22}$$

and

$$\mathscr{H}(u,v;\xi',\eta') = \int\int_{-\infty}^{\infty} H_0(\xi_1,\eta_1)H_0^*(\xi_1+\lambda u,\eta_1+\lambda v)$$
$$\cdot H_0^*(\xi_1+\xi',\eta_1+\eta')H_0(\xi_1+\xi'+\lambda u,\eta_1+\eta'+\lambda v)d\xi_1 d\eta_1 .$$

Clearly, the quantity $\mathscr{M}$ characterizes the atmospheric contribution and $\mathscr{H}$ the telescope contribution to the speckle transfer function.

Further simplification of (7.22) requires that an assumption about the joint probability distribution of the process $A(\xi,\eta)$ be made. The most satisfactory distribution is the log normal, in which the log modulus and phase each have a Gaussian probability density. KORFF [7.29] evaluated the speckle transfer function using this model and results will be shown below; however, neither this model or the zero-scintillation versions of it [7.24] have a simple analytical solution and require extensive numerical calculations.

In order to illustrate in a qualitative way the form of the speckle transfer function, we shall assume that $A(\xi,\eta)$ is a complex Gaussian process [7.30]. This is a poor assumption in good seeing, although it improves as the seeing deteriorates; this assumption also violates the weak scintillation requirement for normalization. For a complex Gaussian process, the fourth-order moment of (7.22) reduces to a product of second-order moments

$$\mathscr{M}(u,v;\xi',\eta') = \langle A(\xi_1,\eta_1)A^*(\xi_1+\lambda u,\eta_1+\lambda v)\rangle$$
$$\cdot\langle A^*(\xi_1+\xi',\eta_1+\eta')A(\xi_1+\xi'+\lambda u,\eta_1+\eta'+\lambda v)\rangle$$
$$+\langle A(\xi_1,\eta_1)A^*(\xi_1+\xi',\eta_1+\eta')\rangle$$
$$\cdot\langle A^*(\xi_1+\lambda u,\eta_1+\lambda v)A(\xi_1+\xi'+\lambda u,\eta_1+\eta'+\lambda v)\rangle ,$$

which, when substituted into (7.22) yields

$$\mathscr{T}(u,v) = |T_s(u,v)|^2 |T_0(u,v)|^2 + \mathscr{S}^{-2} \int\int_{-\infty}^{\infty} |T_s(\xi'/\lambda,\eta'/\lambda)|^2$$
$$\cdot \mathscr{H}(u,v;\xi',\eta')d\xi' d\eta' . \tag{7.23}$$

Now $|T_s(\xi'/\lambda,\eta'/\lambda)|^2$ is of width of order r_0/λ and $\mathscr{H}$ is essentially constant for such values of ξ', η', provided that $\sqrt{u^2+v^2} < (D-r_0)/\lambda$. The second term of (7.23) therefore reduces to

$$\mathscr{S}^{-2} \int\int_{-\infty}^{\infty} |T_s(\xi'/\lambda,\eta'/\lambda)|^2 d\xi' d\eta' \times \mathscr{H}(u,v;0,0) , \tag{7.24}$$

except for $\sqrt{u^2+v^2} > (D-r_0)/\lambda$.

The first integral in (7.24) can be evaluated using (7.17) to give $0.109\pi r_0^2$; the quantity $\mathscr{H}(u,v;0,0)$ is simply

$$\mathscr{H}(u,v;0,0) = \int\int_{-\infty}^{\infty} |H_0(\xi_1,\eta_1)|^2 |H_0(\xi_1+\lambda u,\eta_1+\lambda v)|^2 d\xi_1 d\eta_1 ,$$

which, when multiplied by $\mathscr{S}^{-1}$ is the *diffraction-limited* optical transfer function $T_D(u,v)$ for an unapodized, or clear, pupil; and finally, the remaining $\mathscr{S}^{-1}$ equals $4/\pi D^2$.

Thus the expression for the speckle transfer function reduces to

$$\mathscr{T}(u,v)=|\langle T(u,v)\rangle|^2+0.435(r_0/D)^2T_D(u,v), \tag{7.25}$$

or, defining the number of speckles as

$$N_{sp}=2.3\left(\frac{D}{r_0}\right)^2,$$
$$\mathscr{T}(u,v)=|\langle T(u,v)\rangle|^2+\frac{1}{N_{sp}}T_D(u,v). \tag{7.26}$$

In both equations it is assumed that $\sqrt{u^2+v^2}\leqq(D-r_0)/\lambda$.

The essential feature of the speckle transfer function, (7.25 or 26), is that there is a term proportional to the diffraction-limited optical transfer function, that extends almost up to the diffraction-limited cut-off D/λ; expressions (7.25 and 26) indicate that this result is *independent of telescope aberrations* [7.30], although there is, in fact, a weak dependence on aberrations to be discussed in Sect. 7.2.4. With $D\cong 4$ m and $r_0\cong 0.1$ m,

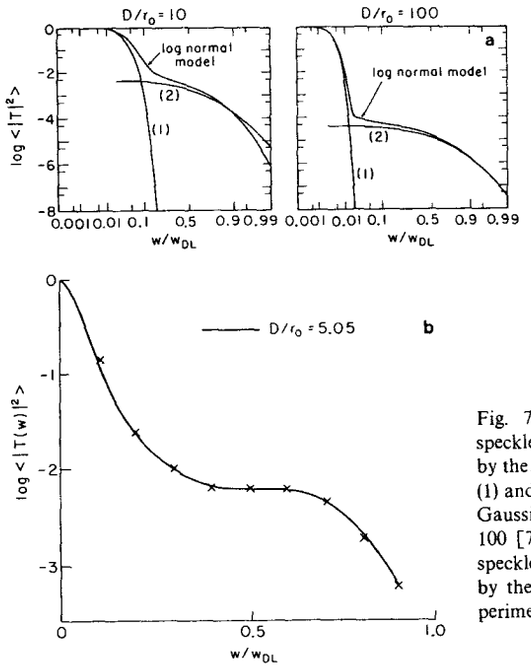

Fig. 7.4. (a) Comparison of the speckle transfer function predicted by the log normal model with terms (1) and (2) of (7.26) for the complex Gaussian model, for $D/r_0=10$ and 100 [7.49]. (b) Comparison of the speckle transfer function predicted by the log normal model with experimental results [7.32]

the number of speckles N_{sp} is approximately 3.7×10^3, indicating that the diffraction-limited information in the image may be carried with a low signal-to-noise ratio. However, the normalization of (7.25, 26) to unity at zero spatial frequency gives a misleading impression of the signal-to-noise ratio which is best evaluated by other methods (Sect. 7.3).

Since (7.25, 26) are based on the assumption that $A(\xi,\eta)$ is a complex Gaussian process, they give only the qualitative behaviour of the transfer function. The speckle transfer function can be calculated using the log normal model and these results are compared to (7.26) in Fig. 7.4a for $D/r_0=10$ and 100 [7.49]; the main differences lie in the region between the low- and high-frequency terms. In fact, at low spatial frequencies, the correct asymptotic form of the speckle transfer function is $|\langle T\rangle_{SE}|^2$, where $\langle T\rangle_{SE}$ is the so called "short-exposure" average [7.22, 29] (i.e., the average when each point image is re-centered). Careful measurements by AIME et al. [7.31] and CHELLI et al. [7.32] are in excellent agreement with the log normal model, particularly if the effect of the central obstruction and the (small) effect of defocus are allowed for. Fig. 7.4b shows the result of a measurement in the infra-red.

7.2.4 Effect of Aberrations

Telescope aberrations have two potential effects on the speckle transfer function. If they are very severe, optical-path differences greater than the coherence length of the light may be introduced and this would lead to a strong attenuation of the transfer function. A proper analysis of this effect requires a detailed consideration of temporally partially coherent imaging; this is not carried out here since the effects in normal circumstances are small, as the following analysis shows.

Consider the simplest aberration—defocus—of magnitude m waves at the edge of the pupil; the longitudinal and angular transverse ray aberrations Δz and $\Delta\alpha$, respectively, are given by

$$\Delta z=\frac{8m\lambda f^2}{D^2}$$
and
$$\Delta\alpha=\frac{8m\lambda}{D}. \tag{7.27}$$

Under most observing conditions, focus can be established to a tolerance $\Delta\alpha$ of less than 1".0, giving a maximum value of m of approximately 5λ for a 4 m telescope. The coherence length l_c of light of bandwidth $\Delta\lambda$ is given

approximately by

$$l_c \cong \frac{\bar{\lambda}^2}{\Delta\lambda}, \tag{7.28}$$

and with typical bandwidths ($\Delta\lambda = 20$ nm, $\bar{\lambda} = 500$ nm) it is clear that $l_c > m\lambda$. In practice, aberrations only introduce path differences greater than the coherence length if the bandwidth is large or the aberrations are severe.

Aberrations also affect the shape of the speckle transfer function in the quasi-monochromatic case; their effect reduces as the ratio D/r_0 increases and disappear in the limit $D/r_0 \to \infty$. The effect of several aberrations was investigated by DAINTY [7.33] using the complex Gaussian model for the atmospheric turbulence. More precise calculations for defocus and astigmatism were made by RODDIER et al. [7.34] using the log normal model and were compared to the measurements of KARO and SCHNEIDERMAN [7.35]. These results are shown in Fig. 7.5; it should be emphasized that the defocus in this case was made artifically large to illustrate the effect, with $m \cong 6.4\lambda$ corresponding to an angular transverse ray aberration (of extremal rays) of $\Delta\alpha \cong 3''.3$.

For aberrations other than defocus, intuitive reasoning based on the approximations necessary to obtain (7.25, 26) suggests that the effect of aberrations is small if the seeing disc is larger than the point spread function due to telescope aberrations alone. Thus, a telescope of poor optical quality achieves *diffraction-limited* angular resolution if sufficiently severe atmospheric turbulence (real or artificially induced) is present [7.30]. Unfortunately, poor seeing (small r_0) also results in a low signal-to-noise ratio (Sect. 7.3).

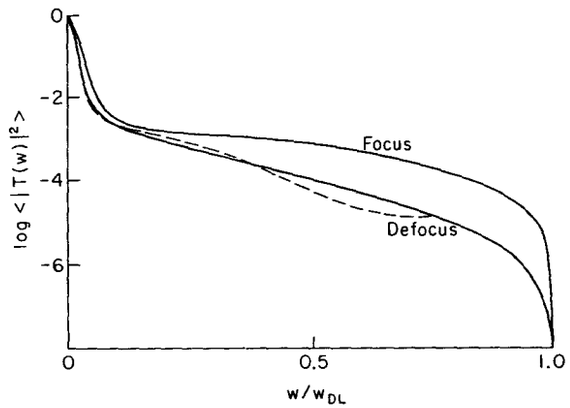

Fig. 7.5. *Solid lines*—theoretical speckle transfer functions for $D/r_0 = 19.2$ in focus and defocused by 6.4λ. *Broken line*—curve observed by Karo and Schneiderman under defocused conditions [7.34]

7.2.5 Effect of Exposure Time

In practice, each image is the result of a finite exposure time Δt, which always has the effect of attenuating the speckle transfer function. Let the instantaneous point spread function at time t be denoted $P(\alpha, \beta, t)$ and the instantaneous transfer function be $T(u, v, t)$. The speckle transfer function for instantaneous exposures ($\Delta t \to 0$) is defined by

$$\mathscr{T}(u, v) \equiv \langle |T(u, v, t)|^2 \rangle, \tag{7.29}$$

whereas for an exposure time Δt it is equal to

$$\mathscr{T}_{\Delta t}(u, v) = \frac{1}{\Delta t^2} \int_0^{\Delta t} \int \langle T^*(u, v, t) T(u, v, t') \rangle dt\, dt' . \tag{7.30}$$

The term $\langle \cdot \rangle$ in (7.30) is called the temporal cross-energy spectrum and plays an important role in time-integration effects. Assuming temporal stationarity of the process $T(u, v, t)$, (7.30) may also be written

$$\mathscr{T}_{\Delta t}(u, v) = \frac{1}{\Delta t} \int_{-\Delta t}^{+\Delta t} \left(1 - \frac{|\tau|}{\Delta t}\right) \langle T^*(u, v, t) T(u, v, t+\tau) \rangle d\tau . \tag{7.31}$$

The finite exposure time speckle transfer function, $\mathscr{T}_{\Delta t}(u, v)$, is always less than (or equal to) the instantaneous transfer function $\mathscr{T}(u, v)$, as the following analysis shows [7.36]. The Schwartz inequality implies that

$$|\langle T^*(u, v, t) T(u, v, t+\tau) \rangle| \leqq \langle |T(u, v, t)|^2 \rangle$$

so that, using (7.31),

$$\begin{aligned} \mathscr{T}_{\Delta t}(u, v) &\leqq \frac{1}{\Delta t} \int_{-\Delta t}^{+\Delta t} \left(1 - \frac{|\tau|}{\Delta t}\right) |\langle T^*(u, v, t) T(u, v, t+\tau) \rangle| d\tau \\ &\leqq \frac{1}{\Delta t} \int_{-\Delta t}^{+\Delta t} \left(1 - \frac{|\tau|}{\Delta t}\right) \langle |T(u, v, t)|^2 \rangle d\tau \\ &= \langle |T(u, v, t)|^2 \rangle \equiv \mathscr{T}(u, v), \end{aligned}$$

i.e.,

$$\mathscr{T}_{\Delta t}(u, v) \leqq \mathscr{T}(u, v). \tag{7.32}$$

This is a general result which is independent of the detailed nature of the turbulence. The magnitude of the attenuation of $\mathscr{T}(u,v)$ due to an exposure time Δt depends, from an experimental point of view, on the form of the temporal cross-energy spectrum $\langle T^*(u,v,t)T(u,v,t+\tau)\rangle$; only qualitative estimates of this function have been reported [7.37].

The temporal cross-energy spectrum is equal to the Fourier transform of the spatially averaged space-time[3] intensity correlation function,

$$\langle T^*(u,v,t)T(u,v,t+\tau)\rangle = \int_{-\infty}^{\infty}\int \left[\int_{-\infty}^{\infty}\int \langle P(a,\beta,t)P(a+\Delta\alpha,\beta+\Delta\beta,t+\tau)\rangle d\alpha\, d\beta\right] \cdot\exp[-2\pi i(u\Delta\alpha+v\Delta\beta)]d\Delta\alpha\, d\Delta\beta\,, \tag{7.33}$$

where $\langle P(\alpha,\beta,t)P(\alpha+\Delta\alpha,\ \beta+\Delta\beta,\ t+\tau)\rangle$ is the space-time cross-correlation function of the instantaneous point spread function. A few measurements of the spatially integrated space-time cross-correlation function have been made [7.38, 39]. They show that, in general, this function is not cross-spectrally pure, so that it cannot be written as the product of two separable functions of (u,v) and t,

$$\langle T^*(u,v,t)T(u,v,t+\tau)\rangle \neq \mathscr{T}(u,v)C(\tau). \tag{7.34}$$

(This result is referred to in Sect. 7.3.3 on the optimum exposure time.)

When $\Delta\alpha=\Delta\beta=0$, the space-time cross-correlation is simply equal to the temporal autocorrelation of the point spread function $\langle P(\alpha,\beta,t)P(\alpha,\beta,t+\tau)\rangle$. Several measurements of this function have been reported [7.38–41] and a sample of results taken at Mauna Kea, Hawaii, are shown in Fig. 7.6; the average correlation time of the image intensity was 15 ms (61 cm telescope). In site testing for new locations for stellar interferometry, it is important to measure both the spatial and temporal properties of seeing.

Although it is the cross-energy spectrum that most directly influences the effect of a finite exposure time Δt, from a more fundamental point of view the important quantity is the fourth order correlation function of the complex amplitude in the pupil:

$$\langle A(\xi,\eta,t)A^*(\xi+\xi_1,\eta+\eta_1,t) \cdot A^*(\xi+\xi_2,\eta+\eta_2,t+\tau)A(\xi+\xi_3,\eta+\eta_3,t+\tau)\rangle \tag{7.35}$$

[3] As given in (7.33), this is an angle-time correlation function; the name space-time is more widely used, distances (x,y) in the image plane being related to angles (α,β) by $x=\alpha f$, $y=\beta f$, where f is the focal length.

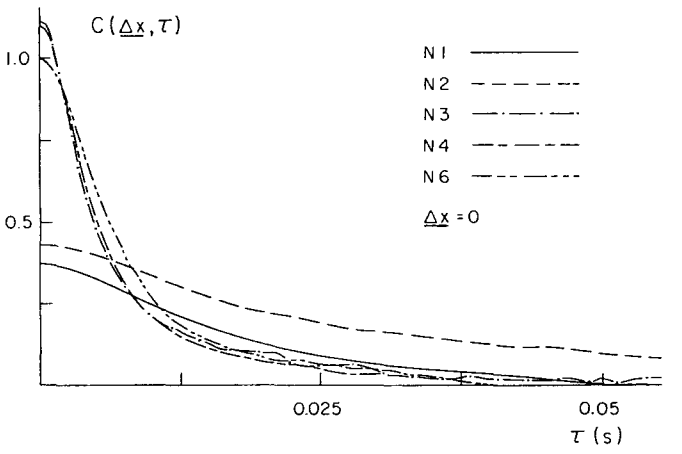

Fig. 7.6. Temporal image intensity autocorrelations over 5 nights at Mauna Kea, Hawaii, measured using a 61 cm telescope [7.39]

[compare with the expression for $\mathscr{M}$ in (7.22)]. For both complex Gaussian and log normal complex amplitude, this fourth order moment is determined by the behaviour of the second order moment. RODDIER and coworkers [7.42, 43] have calculated the effect of a finite exposure time on the speckle transfer function using the log-normal model and the assumption that the complex amplitude $A(\xi,\eta,t)$ moves rigidly across the telescope pupil (the Taylor approximation). For a velocity v along the ξ axis,

$$\langle A(\xi,\eta,t)A^*(\xi+\Delta\xi,\eta+\Delta\eta,t+\tau)\rangle = f(\Delta\xi-v\tau,\Delta\eta), \tag{7.36}$$

For a telescope of diameter D, a velocity v of the turbulence implies a characteristic image time scale of D/v; the results in [7.42] show that the attenuation of the transfer function is not too severe provided that $\Delta t < D/v$.

Spatio-temporal measurements (of $|A|^2$) imply that, in addition to the rigid translation described by (7.36), there is also a strong decorrelation due to "boiling" of $A(\xi,\eta,t)$. This can be explained by a multilayer model for the turbulence [7.24] with a velocity distribution Δv of the atmospheric layers; this leads to a characteristic time scale of $r_0/\Delta v$ and a uniform attenuation of the high-frequency part of the speckle transfer function.

KARO and SCHNEIDERMAN [7.44] have measured the effect of a finite exposure time on the speckle transfer function; their results obtained on

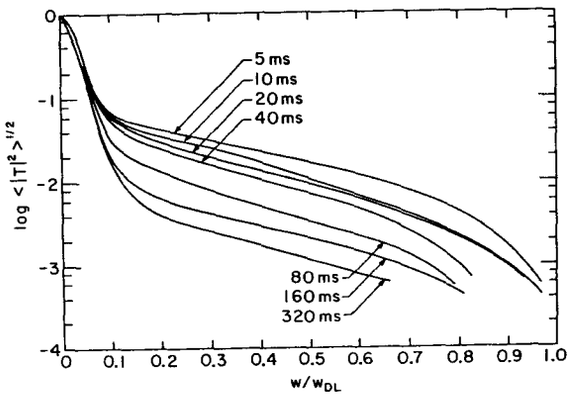

Fig. 7.7 The effect of finite exposure time on the speckle transfer function [7.44]

the 1.6 m telescope at Maui, Hawaii, are shown in Fig. 7.7. Unfortunately, the spatio-temporal atmospheric data required to compare these measurements with theory were not available. However, the uniform attenuation suggests that the wavefront "boiling" dominated over simple rigid translation and implies a time-scale consistent with $r_0/\Delta v \cong 20$ ms.

7.2.6 Effect of Finite Bandwidth

A finite bandwidth $\Delta\lambda$, centered at $\bar{\lambda}$, has two effects both of which attenuate the speckle transfer function. These effects are identical to those observed in polychromatic laboratory-generated Fraunhofer plane speckle patterns discussed in Chap. 3. The two effects are (i) a radial dispersion effect similar to that produced by a grating and (ii) a loss of speckle contrast caused by atmospheric (or, possibly, telescope induced) optical path differences being comparable to the coherence length $l_c \equiv \bar{\lambda}^2/\Delta\lambda$ of the radiation.

In accordance with simple first order grating theory, a spread of wavelengths $\Delta\lambda/\bar{\lambda}$ causes a spread in diffraction angles $\Delta\omega/\bar{\omega}$,

$$\frac{\Delta\omega}{\bar{\omega}} = \frac{\Delta\lambda}{\bar{\lambda}}.$$

Taking $\bar{\omega}$ to be the seeing angle λ/r_0 (7.19), and defining ω_0 to be the angular diameter of a speckle ($\equiv \lambda/D$), we find that the fractional radial

elongation of speckles, $\Delta\omega/\omega_0$ at the seeing angle to be given by

$$\frac{\Delta\omega}{\omega_0} = \frac{\Delta\lambda}{\bar{\lambda}}\frac{D}{r_0}.$$

To determine a criterion for the maximum permissable value of $\Delta\lambda/\bar{\lambda}$, we require that $\Delta\omega/\omega_0 < 1$, yielding

$$\left[\frac{\Delta\lambda}{\bar{\lambda}}\right]_1 < \frac{r_0}{D}. \tag{7.37}$$

In order to calculate a criterion for coherence length effects to be negligible, we require a formula for the root-mean-square optical path fluctuation $\sigma_z(\xi)$ between two points spaced ξ apart in the telescope pupil; the Kolmogorov theory [7.24] predicts that

$$\sigma_z(\xi) \cong 0.42\bar{\lambda}\left(\frac{\xi}{r_0}\right)^{5/6}, \tag{7.38}$$

in which $\sigma_z(\xi)$ is in fact independent of wavelength since $r_0 \propto \lambda^{6/5}$. Thus over a telescope aperture of diameter D we may estimate σ_z by substituting $\xi = D$ in (7.38); requiring that the coherence length $l_c > \sigma_z$, we obtain

$$\left[\frac{\Delta\lambda}{\bar{\lambda}}\right]_2 < 2.4\left(\frac{r_0}{D}\right)^{5/6}. \tag{7.39}$$

Other, more stringent, criteria have been suggested [7.23]. For a typical $r_0 = 0.1$ m and $D = 4$ m, criteria (7.37, 39) yield

$$\left[\frac{\Delta\lambda}{\bar{\lambda}}\right]_1 < 0.025, \quad \left[\frac{\Delta\lambda}{\bar{\lambda}}\right]_2 < 0.111,$$

implying that the chromatic dispersion effect is dominant and that, for $\bar{\lambda} = 500$ nm, the bandwidth $\Delta\lambda$ should be less than 12.5 nm.

Measurements by KARO and SCHNEIDEMAN [7.44] with $D/r_0 \cong 14$ show no discernable effect on the speckle transfer function for $\Delta\lambda/\bar{\lambda} < 0.06$; this is consistent with $[\Delta\lambda/\lambda]_1 < 0.07$ given by criterion (7.37). Even for $\Delta\lambda/\bar{\lambda} \cong 0.14$, the mid-frequencies of $\mathcal{T}(u, v)$ were attenuated by only a factor of two.

Since the chromatic dispersion effect is important, it may be worthwhile to design a relay optical system that removes the dispersion [7.45].

Various optical systems have been suggested for this [7.46], but they suffer by having a very small effective field angle and no design has yet been successfully incorporated into a speckle camera system.

7.2.7 Isoplanicity

If a linear system is non-isoplanatic (i.e., if its point spread function depends on both object and image coordinates), then the elementary convolution relationship of (7.2) is replaced by

$$I(\alpha,\beta)=\int_{-\infty}^{\infty}\int O(\alpha',\beta')P(\alpha-\alpha',\beta-\beta';\alpha',\beta')d\alpha'd\beta', \tag{7.40}$$

where $P(\Delta\alpha,\Delta\beta;\alpha',\beta')$ is the instantaneous point spread function for an object point at (α',β'). There is now no meaningful concept of an instantaneous transfer function or a speckle transfer function. However, defining $T(u,v;\alpha',\beta')$ to be the Fourier transform of $P(\alpha-\alpha',\beta-\beta';\alpha',\beta')$ with respect to the variables (α,β), the average image energy spectrum $\Phi_I(u,v)$ reduces to

$$\Phi_I(u,v)\equiv\langle|i(u,v)|^2\rangle=\int_{-\infty}^{\infty}\int C_O(\alpha_1,\beta_1)\langle T(u,v;\alpha',\beta')\cdot T^*(u,v;\alpha'-\alpha_1,\beta'-\beta_1)\rangle\exp[-2\pi i(u\alpha_1+v\beta_1)]d\alpha_1 d\beta_1, \tag{7.41}$$

where $\alpha_1=\alpha-\alpha'$ and $\beta_1=\beta-\beta'$.

If the function $T(u,v;\alpha',\beta')$ is independent of the object point (α',β'), i.e. the imaging is isoplanatic, then (7.41) simplifies to the usual result.

$$\Phi_I(u,v)=\Phi_O(u,v)\langle|T(u,v)|^2\rangle. \tag{7.7}$$

However, according to (7.41), there is no longer a simple relationship between object and image properties, and the form of the cross-spectrum,

$$\langle T(u,v;\alpha',\beta')T^*(u,v;\alpha'-\alpha_1,\beta'-\beta_1)\rangle$$

between speckle patterns produced by two point sources separated by angle (α_1,β_1) plays an important role.

KORFF et al. [7.47], SHAPIRO [7.48], and FRIED [7.49] have investigated this problem using the log-normal model for atmospheric turbulence. However, a more complete analysis can be carried out if the complex Gaussian model of the wavefront $A(\xi,\eta)$ is used, as shown by RODDIER et al. [7.50]. Using a multiple-layer model for the turbulence,

they estimate the "atmospheric isoplanatic angle" $\delta\omega$ to be given by

$$\delta\omega\cong 0.36\frac{r_0}{\Delta h}, \tag{7.42}$$

where Δh is a measure of the altitude dispersion of the turbulent layers [7.50]. This simple relationship does not reveal the fact that high angular frequencies decorrelate more rapidly than lower ones as the angle of separation (α_1,β_1) increases, but gives a good estimate of the extent of the isoplanatic region. Based on measured profiles of the variation of turbulence with altitude (see Vernin in [7.42]), predicted isoplanatic angles were in the range 1".9 to 5".4 over six nights at Haute Provence Observatory, with an average of 3".1 [7.50].

Several measurements of the isoplanatic angle or related quantities have been reported [7.37, 51–53]. The values vary widely, the most reliable quantitative estimates being in the range 1".5–5".0 [7.51, 52], i.e. the same order of magnitude as the theoretical predictions. Qualitative estimates, based on the successful implementation of speckle holography [7.37, 53], indicate some correlation of image intensity for stars as far apart as 22".0.

7.2.8 Self-Calibration of Speckle Interferometry

In order to recover the energy spectrum of the object $\Phi_O(u,v)$, the average energy spectrum of the image $\Phi_I(u,v)$ is divided by the speckle transfer function

$$\Phi_O(u,v)=\Phi_I(u,v)/\mathcal{T}(u,v). \tag{7.43}$$

In practice, the speckle transfer function is estimated by finding the average energy spectrum for a point source (or reference star). Unfortunately, as we have seen in previous sections, the speckle transfer function depends on a number of atmospheric parameters (such as r_0 and time scale) and these parameters themselves vary considerably over both short (~seconds) and long (~hours) periods of time. Under stable atmospheric conditions, application of (7.43) is straightforward, but under (more typical) unstable conditions, the use of (7.43) can lead to considerable errors in the estimation of the object's spectrum. This is less critical for measurements of simple structural features of an object (e.g., the vector separation of a binary star) but crucial for photometric features (e.g., magnitude difference of a binary star).

Two approaches to this problem have been suggested. The first is to make simultaneous measurements of r_0 and use the established theory to

predict the form of the speckle transfer function [7.24]. The measurements of AIME et al. [7.31] and CHELLI et al. [7.32] suggest that the instantaneous ($\Delta t \to 0$), narrowband ($\Delta\lambda \to 0$) speckle transfer function can be predicted for an aberration-free telescope, but in practice focussing errors, aberrations, the finite exposure time and other effects may influence it. Nevertheless, this appears to be a promising technique, particularly in the infra-red where the second approach is less reliable.

The second approach, originally suggested by WORDEN and coworkers [7.54, 55], involves subtracting the cross-correlation of uncorrelated images from the autocorrelation of individual frames. Let $I(\alpha, \beta)$ be an instantaneous short-exposure image and $I'(\alpha, \beta)$ be another instantaneous short-exposure image taken some time after the first one so as to be uncorrelated with it; then, denoting the result by $C_I'(\alpha, \beta)$,

$$C_I'(\alpha,\beta) = \langle I(\alpha,\beta) * I(\alpha,\beta)\rangle - \langle I(\alpha,\beta) * I'(\alpha,\beta)\rangle . \tag{7.44}$$

In fact, no second image is required, since (7.44) is exactly the same as [7.56]

$$C_I'(\alpha,\beta) = \langle I(\alpha,\beta) * I(\alpha,\beta)\rangle - \langle I(\alpha,\beta)\rangle * \langle I(\alpha,\beta)\rangle , \tag{7.45}$$

i.e. the average of the angular autocorrelation minus the autocorrelation of the average image.

These equations may equally well be written in the angular frequency domain, giving a resultant image energy spectrum $\Phi_I'(u, v)$,

$$\Phi_I'(u,v) = \Phi_O(u,v)\mathscr{T}'(u,v) , \tag{7.46}$$

where the transfer function for this technique is given by

$$\mathscr{T}'(u,v) = \langle |T(u,v)|^2\rangle - |\langle T(u,v)\rangle|^2 . \tag{7.47}$$

The original hypothesis [7.45] was that the shape of $\mathscr{T}'(u, v)$ is independent of atmospheric seeing, and this is correct for the complex gaussian model of the pupil amplitude $A(\xi, \eta)$, as can be seen by substituting (7.26) into (7.47):

$$\mathscr{T}'(u,v) = \frac{1}{N_{sp}} T_D(u,v) , \tag{7.48}$$

where N_{sp} is the number of speckles ($\equiv 2.3(D/r_0)^2$), and $T_D(u, v)$ is the diffraction-limited transfer function.

Two factors combine to invalidate this result for the lower angular frequencies. First, as remarked upon earlier, the asymptotic form of the low frequency dependence of the speckle transfer function is $|\langle T(u,v)\rangle_{SE}|^2$, where $\langle T\rangle_{SE}$ is the average transfer function of centroided (tilt-removed) images; this could be taken into account, in principle, by centroiding each image [7.56] or by other methods [7.57].

Second, the additive form (7.26) of the speckle transfer function is not predicted by the more accurate log-normal model, and the end result is to invalidate this method for frequencies (u, v) less than approximately the seeing limit, i.e. $(u,v) \leqq r_0/\lambda$ [7.55, 58]. When D/r_0 is large, say >10, the seeing-limited frequencies constitute only a small fraction of the available frequency plane and this method may be the most satisfactory way of self-calibration. But in the infra-red, where $D/r_0 < 10$, it is not appropriate.

7.3 Signal-to-Noise Ratio

In the visible region of the spectrum, the signal-to-noise ratio of a measurement and the limiting magnitude of speckle interferometry are ultimately determined by the fluctuations imposed by the atmospheric turbulence and the quantum nature of radiation. Although early film-based speckle cameras were limited by other types of noise, the improvement in detector technology over the past decade has made available detectors that are photon-noise limited [7.59]. Thus in this section we shall discuss only the fundamental noise sources relevant to visible light speckle interferometry (the infra-red case is discussed in Sect. 7.5.2).

Let Q be some quantity that is to be estimated by speckle interferometry; Q may be (a) a point in the energy spectrum $\Phi_O(u, v)$ of the object, (b) a point in the autocorrelation function $C_O(\alpha, \beta)$ of the object, or (c) a parameter derived from the autocorrelation function or energy spectrum, such as the diameter of a star, binary separation or magnitude difference.

We define the signal-to-noise ratio, SNR, of this measurement as

$$\text{SNR} \equiv \frac{\text{expected value of quantity}}{\text{standard deviation of estimate}} ,$$

or

$$\text{SNR} \equiv \frac{\langle Q\rangle}{[\text{var}(Q)]^{1/2}} , \tag{7.49}$$

where $\mathrm{var}(Q) \equiv \langle Q^2 \rangle - \langle Q \rangle^2$ is the variance of Q. In the analysis that follows, the SNRs relate to an estimate of Q based on a single frame of data. Normally, one would take M frames of data and, provided these are statistically independent, the overall SNR for the M frames $(\mathrm{SNR})_M$, is simply given by

$$(\mathrm{SNR})_M = \mathrm{SNR} \cdot M^{1/2} . \tag{7.50}$$

The signal-to-noise ratio is the inverse of the relative error of measurement and in a given astronomical application we would normally be interested in the relative error on some parameter (such as diameter), as in (c). However, each problem has its own specific parameters of interest and to keep our results as general as possible we shall consider the SNR of the energy spectrum or autocorrelation function.

Several investigations of the SNR of a measurement of the autocorrelation function have been made [7.33, 57, 60–63] and the review in the first edition of this volume [7.12] outlines this approach. However, it has been shown [7.64] that the autocorrelation and energy spectrum approaches give exactly equivalent signal-to-noise ratios, although the detailed expressions show little apparent similarity. The decision whether to use the autocorrelation method or the energy spectrum method of data reduction should be based on operational considerations and not on SNR considerations. Thus in the following subsection we evaluate only the SNR of the energy spectrum of the object.

7.3.1 Signal-to-Noise Ratio (SNR) at a Point in the Energy Spectrum

The SNR at a point in the energy spectrum was first evaluated by RODDIER [7.65] and subsequently in more detail by several authors [7.66–69] and reviewed in detail in [7.70]. In this analysis we shall use one-dimensional notation for simplicity, and it is convenient to deal with energy spectra of the image and object that are normalized to unity at zero angular frequency, denoted by $\hat{\Phi}_\mathrm{I}(u)$ and $\hat{\Phi}_\mathrm{O}(u)$, respectively. These are related in the usual way,

$$\hat{\Phi}_\mathrm{I}(u) = \hat{\Phi}_\mathrm{O}(u) \mathscr{T}(u) , \tag{7.51}$$

where the speckle transfer function $\mathscr{T}(u)$ in the frequency range of interest is given by (7.26):

$$\mathscr{T}(u) = \frac{1}{N_{sp}} T_\mathrm{D}(u) , \quad \frac{r_0}{\lambda} < u < \frac{(D - r_0)}{\lambda} . \tag{7.26}$$

We model the jth image, $D_\mathrm{j}(\alpha)$, as an inhomogeneous or compound Poisson process which has a rate proportional to the classical image intensity $I_\mathrm{j}(\alpha)$, i.e.,

$$D_\mathrm{j}(\alpha) = \sum_{\mathrm{k}=1}^{N_\mathrm{j}} \delta(\alpha - \alpha_{\mathrm{jk}}) ,$$

where each delta function represents a detected photon event, α_{jk} is the location of the kth event in the jth frame and N_j is the number of detected photons in the jth frame. In an observation, the squared modulus of the Fourier transform $|d_\mathrm{j}(u)|^2$ is computed for each frame. It is straightforward to show that the average of this is given by [7.66]

$$\langle |d_\mathrm{j}(u)|^2 \rangle = \bar{N}^2 \hat{\Phi}_\mathrm{I}(u) + \bar{N} , \tag{7.52}$$

where $\bar{N}$ is the average number of detected photons per frame. It follows that the energy spectrum of the photon data, $\langle |d_\mathrm{j}(u)|^2 \rangle$, is a biased estimate of $\hat{\Phi}_\mathrm{I}(u)$ to the presence of the $\bar{N}$ term; in the realistic case in which the photon events are not delta functions but have a unit volume spread function $S(\alpha)$, the second term would be $\bar{N}|s(u)|^2$.

There are two estimators Q whose average yield an unbiased estimate of the image energy spectrum. One possibility is to subtract the average number $\bar{N}$ from each $|d_\mathrm{j}(u)|^2$,

$$Q_1 = |d_\mathrm{j}(u)|^2 - \bar{N} , \tag{7.53}$$

and the second possibility is to subtract the actual number N_j,

$$Q_2 = |d_\mathrm{j}(u)|^2 - N_\mathrm{j} . \tag{7.54}$$

In either case, the average values of Q are unbiased estimators,

$$\langle Q_1 \rangle = \langle Q_2 \rangle = \bar{N}^2 \hat{\Phi}_\mathrm{I}(u) . \tag{7.55}$$

For the first estimator, the variance is equal to [7.67]

$$\mathrm{var}(Q_1) = \bar{N} + \bar{N}^2 + 2(2+N) N^3 \hat{\Phi}_\mathrm{I}(u) + \bar{N}^2 \hat{\Phi}_\mathrm{I}(2u) + \bar{N}^4 \hat{\Phi}_\mathrm{I}^2(u) . \tag{7.56}$$

As in all problems of this type, the fluctuation at frequency u is influenced by the value of the energy spectrum at frequency $2u$. At exceedingly low light levels $\bar{N} \ll 1$ (probably of no practical interest!), the SNR per frame for estimate Q_1 is, using (7.49, 55 and 56),

$$\mathrm{SNR} = \bar{N}^{3/2} \hat{\Phi}_\mathrm{I}(u) , \quad \bar{N} \ll 1 . \tag{7.57}$$

The use of definition (7.53) for the estimate Q_1 has the disadvantage that the noise associated with Q_1 contains a contribution arising from N_j, the actual number of photons per frame. These fluctuations are related to the brightness of the object and not to its structure. If one is interested in the morphology of the object, Q_2 is a better estimate; its variance is given by [7.69]

$$\text{var}(Q_2) = \bar{N}^2 + \bar{N}^2\hat{\Phi}_I(2u) + 2\bar{N}^3\hat{\Phi}_I(u) + \bar{N}^4\hat{\Phi}_I^2(u). \tag{7.58}$$

If we consider only frequencies $u > \frac{1}{2}D/\lambda$, the second term in (7.58) can be ignored, yielding a SNR per frame of

$$\text{SNR} = \frac{\bar{N}\hat{\Phi}_I(u)}{1 + \bar{N}\hat{\Phi}_I(u)}. \tag{7.59}$$

Equation (7.59) is the general expression for the signal-to-noise ratio at any point ($u > \frac{1}{2}D/\lambda$) in the energy spectrum of the image. If the speckle transfer function is known exactly (this is never true in practice), then (7.59) is also the SNR at a point in the energy spectrum of the object. Substituting (7.26, 51) into (7.59), and defining the average number of detected photons per speckle $\bar{n}$ as

$$\bar{n} \equiv \frac{\bar{N}}{N_{sp}} = \frac{\bar{N}}{2.3}\left(\frac{r_0}{D}\right)^2, \tag{7.60}$$

we find that the SNR per frame becomes

$$\text{SNR} = \frac{\bar{n}T_D(u)\hat{\Phi}_O(u)}{1 + \bar{n}T_D(u)\hat{\Phi}_O(u)}. \tag{7.61}$$

Two limiting cases are of interest: very bright objects and very faint ones.

(i) For very bright objects, such that

$$\bar{n}T_D(u)\hat{\Phi}_O(u) \gg 1,$$

then,

$$\text{SNR} \cong 1. \tag{7.62}$$

Note that the SNR per frame cannot exceed unity in speckle interferometry and this is one of the disadvantages of the speckle technique, compared to pupil plane interferometry, for bright objects.

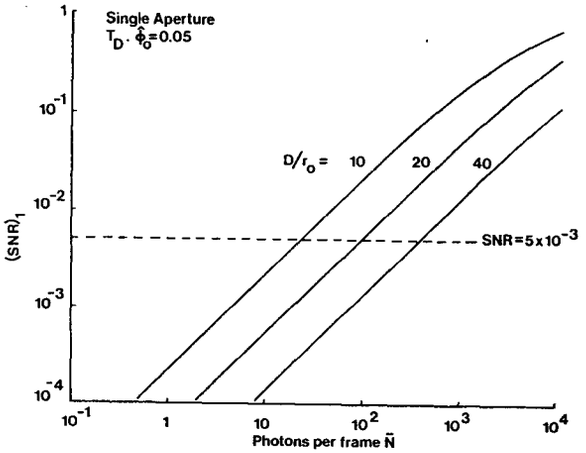

Fig. 7.8. The variation of SNR per frame with the average number of detected photons per frame $\bar{N}$ for $D/r_0 = 10$, 20, and 40, for $T_D\hat{\phi}_0 = 0.05$ [7.70]

(ii) For very faint objects, such that

$$\bar{n}T_D(u)\hat{\Phi}_O(u) \ll 1$$

then

$$\begin{aligned}\text{SNR} &\cong \bar{N}\hat{\Phi}_I(u) \\ &\cong \bar{n}T_D(u)\hat{\Phi}_O(u),\end{aligned} \tag{7.63}$$

where, as before, $\bar{N}$ is the average number of detected photons per frame and $\bar{n}$ is the average number per speckle. This particularly simple formula for the SNR per frame at a point ($u > \frac{1}{2}D/\lambda$) in the energy spectrum of the object is in practice valid for all fainter objects.

An example of the variation of SNR per frame as a function of $\bar{N}$ is shown in Fig. 7.8 for $D/r_0 = 10$, 20, and 40. For faint objects, the SNR is proportional to r_0^2, so that there is a strong dependence of SNR on the seeing. On the other hand, since the average number of photons per speckle (7.60) is independent of telescope diameter, the SNR at a point in the energy spectrum is also independent of telescope diameter, for faint objects. Of course, a larger telescope yields more independent points in the energy spectrum.

7.3.2 Optimum Exposure Time

In the low-light-level case, the SNR at a point in the energy spectrum for M statistically independent frames is, from (7.50, 63),

$$(\mathrm{SNR})_M \cong \sqrt{M\bar{N}}\,\hat{\Phi}_1(u). \tag{7.64}$$

It appears at first sight that a larger exposure time (i.e., increasing $\bar{N}$) leads to a higher SNR; however, this is true only up to an optimum exposure time, after which the decrease in M and $\hat{\Phi}_1(u)$ dominates. The optimum exposure time has been evaluated by WALKER [7.62], and O'DONNELL and DAINTY [7.71].

Let the exposure time be denoted by Δt, the experiment time by T_e and the photon rate by $\mu \equiv \bar{N}/\Delta t$; then, assuming that neighboring exposures are always statistically independent[4] (7.64) can be re-written as

$$(\mathrm{SNR})_M \cong \mu\sqrt{T_e \Delta t}\,\hat{\Phi}_{1,\Delta t}(u), \tag{7.65}$$

where $\hat{\Phi}_{1,\Delta t}(u)$ is the measured image energy spectrum for an exposure time Δt. The temporal behaviour of the image intensity has been discussed in Sect. 7.2.5; there we showed that the measured image energy spectrum may always be written, see (7.31),

$$\hat{\Phi}_{1,\Delta t}(u) = \frac{1}{\Delta t}\int_{-\Delta t}^{\Delta t}\left(1-\frac{|\tau|}{\Delta t}\right)\langle i^*(u,t)i(u,t+\tau)\rangle d\tau. \tag{7.66}$$

Both theory and experiment show that, in general, the cross-spectrum $\langle i^*(u,t)i(u,t+\tau)\rangle$ is *not* separable. On the other hand, measurements [7.39] indicate that the approximation, see (7.34),

$$\langle i^*(u,t)i(u,t+\tau)\rangle \cong \hat{\Phi}_1(u)C(\tau) \tag{7.67}$$

may not be unreasonable under typical observing conditions; in (7.67), $\hat{\Phi}_1(u)$ is the normalized instantaneous energy spectrum and $C(\tau)$ is the normalized temporal autocorrelation function of the stellar image (some measurements are shown in Fig. 7.6). Substituting (7.66, 67) into (7.65) we obtain

$$(\mathrm{SNR})_M \cong \hat{\Phi}_1(u)2\mu\sqrt{\frac{T_e}{\Delta t}}\int_0^{\Delta t}\left(1-\frac{|\tau|}{\Delta t}\right)C(\tau)d\tau. \tag{7.68}$$

[4] Clearly, neighboring exposures cannot be statistically independent unless $\Delta t \gg$ correlation time of the image intensity; when there are only a small number of detected photons per frame, however, there is an approximate statistical independence for neighboring frames.

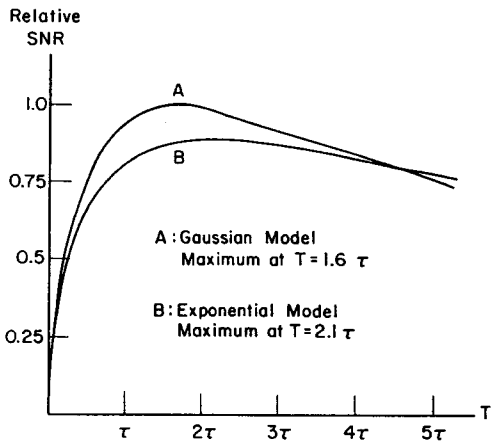

Fig. 7.9. Relative SNR at a point in the power spectrum as a function of the length of the individual short exposures for two models of the time-correlation of the image intensity. The overall time of observation is assumed to be constant and it is also assumed that the average number of detected photons per speckle is very much less than one [7.71]

In Fig. 7.9, the SNR is plotted as a function of exposure time for two models of the temporal correlation function $C(\tau)$, Gaussian and negative exponential, each having a 1/e correlation time of τ_c; the Gaussian model appears to give a better fit to the experimental data of Fig. 7.6. It can be seen that the overall SNR is highest for exposure times Δt equal to $1.6\tau_c$ for the Gaussian model and $2.1\tau_c$ for the exponential one. This is somewhat larger than might be expected and certainly much larger than desirable at high light levels where photon noise is negligible. Since the SNR decreases rather slowly for exposure times longer than $\cong 2\tau_c$, we can also conclude that, if there is some doubt as to the value of τ_c, longer rather than shorter exposures should be used.

7.3.3 Limiting Magnitude

LABEYRIE concluded his original paper on speckle interferometry [7.6] with the comment that "the technique appears to be limited to objects brighter than $m_v = 7$". It was quickly recognized by LABEYRIE and others that, in fact, the faintest objects that can be resolved by this technique are a factor of 10^5 fainter, of apparent visual magnitude $m_v \cong 20$.

Any estimate of the limiting or just-observable magnitude depends on the criterion adopted for "just-observable" as well as on the usual

parameters such as detector quantum efficiency, bandwidth, exposure time and so on. Three examples are given below: an estimate of the complete object energy spectrum, the detection of a binary star, and the measurement of the diameter of a star. In each case we define a factor F to be the product of the exposure time Δt[s], the optical bandwidth $\Delta\lambda$[nm] and the quantum efficiency q of the detector,

$$F \equiv \Delta t \Delta \lambda q . \tag{7.69}$$

We also use the fact that a source of apparent visual magnitude m_v gives rise to an average number of detected photons per m^2 per frame, $\bar{N}_A$, of [7.72]

$$\bar{N}_A = F\, 10^{(8-0.4m_v)} . \tag{7.70}$$

Estimation of the Object Energy Spectrum

At low light levels, combination of (7.50, 63 and 70) gives a SNR of

$$(\mathrm{SNR})_M = M^{1/2} \frac{\pi D^2}{4} F\, 10^{(8-0.4m_v)} \left[0.435 \left(\frac{r_0}{D}\right)^2\right] \hat{\Phi}_O(u) T_D(u) ,$$

which can be re-arranged to give [7.70]

$$m_v = 18.8 + 2.5 \log F - 2.5 \log(\mathrm{SNR})_M + 1.25 \log M + 2.5 \log[\hat{\Phi}_O(u) T_D(u)] + 5 \log r_0 . \tag{7.71}$$

For $r_0 = 0.1$ m, $M = 10^5$, $\Delta t = 0.02$ s, $\Delta\lambda = 25$ nm, $q = 0.1$, $\hat{\Phi}_O(u) T_D(u) = 0.2$ and a limiting $(\mathrm{SNR})_M = 5$, (7.71) predicts a limiting apparent visual magnitude of approximately $m_v = 13.3$, corresponding to approximately 300 detected photons per frame in a 4 m telescope. Note that the limiting magnitude defined in this way is independent of telescope diameter and depends quite strongly on the seeing parameter r_0; in fact, the dependence on r_0 is stronger than (7.71) indicates since the bandwidth and exposure time both change with r_0 [7.23] (Sects. 7.2.5, 6). The value $m_v = 13.3$ is a conservative estimate of the limiting magnitude for many purposes, since it is based on the criterion that the SNR have the value 5 at every point in the energy spectrum.

Detection of Binary Stars

Using a formula for the SNR based on the autocorrelation approach [7.61, 70], in which the estimated quantity is the height of the binary star autocorrelation peak above its local background, we can derive the following limiting magnitude for a binary whose components are equally bright:

$$m_v = 17.3 + 2.5 \log F - 2.5 \log(\mathrm{SNR})_M + 1.25 \log M + 2.5 \log D + 2.5 \log r_0 . \tag{7.72}$$

Substituting the same parameters as above now leads to a limiting magnitude $m_v = 17.6$, corresponding to approximately 5 detected photons per frame an average. By increasing the number of independent frames to 10^6 and slightly increasing the exposure time and bandwidth, binaries as faint as $m_v = 20$ should be observable.

The limiting magnitude predicted by (7.72) has been effectively achieved by HEGE et al. [7.73] in their measurement of the 16.2 magnitude component of the triple quasar PG 1115+08 using approximately 20,000 independent frames.

Estimation of Object Diameter

WALKER [7.57] has made a comprehensive study of the accuracy with which the diameter of an object can be estimated by speckle interferometry, assuming a known limb darkening profile of the star. His results are summarized in Fig. 7.10 for a collection of observing parameters that are similar (but not identical) to the previous two cases. For 1% statistical error in a diameter whose value is 0.″5, the limiting magnitude is approximately $m_v = 16$. Of course, other deterministic effects such as those due to atmospheric calibration are not included in this or previous cases.

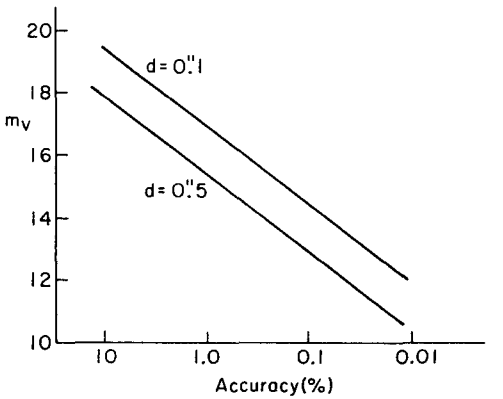

Fig. 7.10. Limiting magnitude m_v as a function of the desired fractional accuracy for a typical set of observing parameters on a 4 m-class telescope (observing period: 2000 s) [7.58]

7.3.4 Space-Time Speckle Interferometry

In the analysis of the optimum exposure time in Sect. 7.3.2, we found that exposures as long as twice the temporal correlation time of the image could be optimum from the point of view of signal-to-noise ratio. Such long exposure times result in attenuation of the high angular frequency components in the measured energy spectrum, and those remain uncorrected. Another drawback of the straightforward speckle method is that no use is made of the fact that photons detected at the end of one exposure are associated with essentially the same classical intensity as those detected at the beginning of the next exposure; thus there is a potential loss of information.

"Space-time" speckle interferometry [7.71, 74] is an extension of speckle interferometry that includes correlations in the time domain as well as in the spatial or angular domain. In one such scheme, the temporal cross-energy spectrum $\langle i^*(u,v,t)i(u,v,t+\tau)\rangle$ is estimated and used to find an estimate of $\hat{\Phi}_I(u,v)$ that is not biased by the effects of a finite exposure time. However, the signal-to-noise ratio of this technique does not appear to be any higher than that associated with the "optimum exposure time" method [7.71]. It does not appear to be worthwhile implementing space-time speckle interferometry unless other benefits can be found (such as obtaining object maps [7.74]).

7.4 Reconstruction of the Object Intensity

The fundamental equation of speckle interferometry relates the average energy spectrum of the image $\Phi_I(u,v)$ to that of the object $\Phi_O(u,v)$,

$$\Phi_I(u,v)=\Phi_O(u,v)\mathscr{T}(u,v), \tag{7.7}$$

where $\mathscr{T}(u,v)$ is the speckle transfer function. Under favorable conditions this equation can be inverted to yield an estimate of the object energy spectrum

$$\Phi_O(u,v)\equiv|o(u,v)|^2 = \left|\int_{-\infty}^{\infty}\int O(\alpha,\beta)\exp[-2\pi i(\alpha u+\beta v)]d\alpha\,d\beta\right|^2, \tag{7.73}$$

where $O(\alpha,\beta)$ is the angular distribution of object intensity and $o(u,v)$ is its Fourier transform. It should be noted that, by the van Cittert-Zernike theorem [7.2], $o(u,v)$ is a spatial coherence function (strictly, the mutual intensity) and $|o(u,v)|$ is often called a visibility function.

It is impossible, *in general*, to calculate a unique object intensity $O(\alpha,\beta)$ from a knowledge of only its energy spectrum $\Phi_O(u,v)$; this simple fact cannot be stressed too strongly. In some special cases, unique reconstruction of $O(\alpha,\beta)$ is possible; in a second set of special cases, unique reconstructions can be formed almost always; and in a third set of special cases, additional information is available that enables a unique solution to be found.

The object energy spectrum $\Phi_O(u,v)$ contains no obvious information about the phase of the Fourier transform of $O(\alpha,\beta)$ and for this reason the problem of reconstructing the object intensity from $\Phi_O(u,v)$ is referred to as the "phase problem". Phase problems arise in many branches of physics—scattering, x-ray diffraction, coherence theory and microscopy—and a detailed review is beyond the scope of this chapter (see [7.75, 76]). Our review will be strictly limited to the phase problem as it occurs in the measurement of angular coherence functions by stellar speckle interferometry; short reviews of this may be found in [7.12–15, 77] and a comprehensive review was given by BATES [7.11]. It is interesting to note that some of the earliest work on the phase problem by Lord RAYLEIGH [7.78] and, in the modern era, by WOLF [7.79] was also concerned with coherence theory.

The plan of this section is as follows. In Sect. 7.4.1 we discuss the basic reason for the ambiguity of the phase problem. The next two Sects. 7.4.2, 3 deal with attempts at object reconstruction from the energy spectrum only, whilst in Sects. 7.4.4–7 we describe other methods that incorporate information in addition to the energy spectrum. The subject is summarized in Sect. 7.4.8. The review is limited to the speckle method of stellar interferometry; in this regard it should be noted that there is increasing evidence [7.9, 80–82] that other methods of stellar interferometry are probably more appropriate for object reconstruction.

7.4.1 Ambiguity of the Phase Problem

An essentially theoretical restriction in the phase problem, which is always satisfied in practice, is that the object intensity $O(\alpha,\beta)$ has a finite angular extent with support (2a, 2b); thus $o(u,v)$ is the *finite* Fourier transform,

$$o(u,v)=\int_{-a}^{a}\int_{-b}^{b} O(\alpha,\beta)\exp[-2\pi i(u\alpha+v\beta)]d\alpha\,d\beta\,. \tag{7.74}$$

It can be shown that the analytic continuation of $o(u,v)$ to the complex plane, $o(z_1,z_2)$ where z_1, z_2 are complex variables, is an entire function of

exponential type. Such functions are completely specified by their (complex) zeros. The zeros provide a unifying concept for the study of all phase retrieval methods; their importance in interferometry was discussed by BATES [7.83] and in a more general context by ROSS and colleagues [7.85–87]. Although the zeros are the unifying concept, they are not necessarily of practical value in computer-based algorithms due to the complexity of determining their locations.

Before discussing the reason for the ambiguity of the phase problem, we should note that certain phase ambiguities do not affect the form of the object intensity and are ignored in the following analysis. Defining the phase of $o(u,v)$ as phase $\{o(u,v)\}$, we are not concerned with the following variants:

$$\text{phase } \{o(u,v)\}+\phi, \text{ where } \phi \text{ is a constant,} \tag{7.75a}$$

$$\text{phase } \{o(u,v)\}+2\pi(u\alpha_1+v\beta_1), \text{ where } (\alpha_1,\beta_1) \text{ is a constant vector,} \tag{7.75b}$$

$$-\text{ phase } \{o(u,v)\}. \tag{7.75c}$$

The addition of a constant phase, (7.75a), does not alter the object intensity $O(\alpha,\beta)$; the second variant, (7.75b), leads to a shifted object $O(\alpha+\alpha_1,\beta+\beta_1)$; the third case, (7.75c), gives $O(-\alpha,-\beta)$, which is a 180° rotated version of the object. In the discussion below, these trivial ambiguities are ignored.

Our approach to describing the phase problem is, following BRUCK and SODIN [7.88], to represent the object by a finite number of samples, equally spaced (for simplicity) by Δ on a grid of $(N+1)$ by $(M+1)$ points. Defining new complex variables w_1 and w_2

$$w_1=\exp(-2\pi i z_1\Delta), \quad w_2=\exp(-2\pi i z_2\Delta), \tag{7.76}$$

the Fourier transform $o(w_1,w_2)$ can be written as a finite polynomial in w_1 and w_2

$$o(w_1,w_2)=w_1^{-a/\Delta}w_2^{-b/\Delta}\sum_{n=0}^{N}\sum_{m=0}^{M}O(n\Delta-a,m\Delta-b)w_1^n w_2^m.$$

The terms $w_1^{-a/\Delta}$ and $w_2^{-b/\Delta}$ merely define the (α,β) origin; ignoring these, and simplifying the notation we write

$$o(w_1,w_2)=\sum_{n=0}^{N}\sum_{m=0}^{M}O_{nm}w_1^n w_2^m. \tag{7.77}$$

The most important feature of (7.77) is that the (discrete) Fourier transform of the object intensity can be written as a finite polynomial in the complex variables w_1 and w_2, the coefficients of the polynomial being the sampled values of the object intensity. In this approach to the phase problem, the mathematics of polynomials is important; note, however, that this approach is less general than required by the original problem, which was for continuous, not discrete, object functions.

Consider now the one dimensional case,

$$o(w_1)=\sum_{n=0}^{N}O_n w_1^n. \tag{7.77a}$$

A one-dimensional polynomial can always be factorized, or reduced, into prime factors,

$$o(w_1)=C\prod_{j=1}^{N}(w_1-w_{1,j}), \tag{7.78}$$

where C is a constant and $w_{1,j}$ are the roots or zeros. The N zeros and the constant C completely determine the Fourier transform $o(w_1)$ and hence the object O_n. If the object is real, as in the present case, the zeros lie on the unit circle or in complex conjugate pairs around the unit circle and only $N/2$ zero locations are required to specify the object; positivity

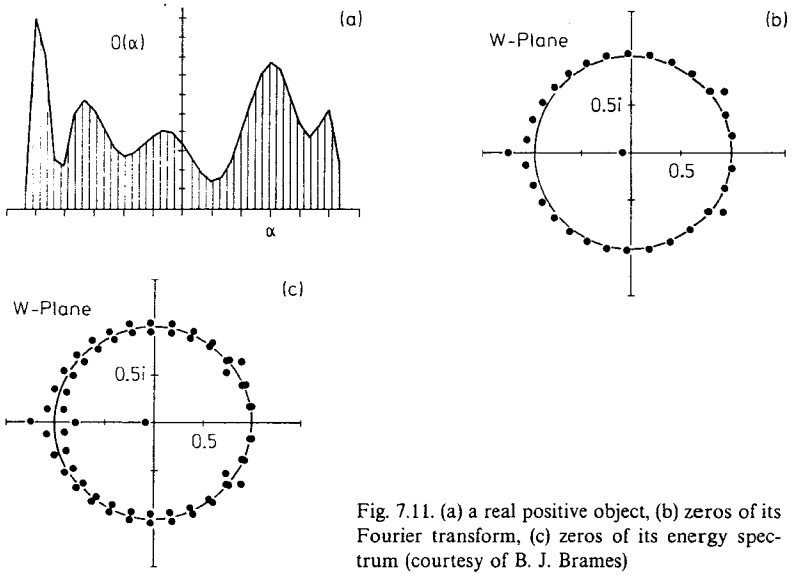

Fig. 7.11. (a) a real positive object, (b) zeros of its Fourier transform, (c) zeros of its energy spectrum (courtesy of B. J. Brames)

requires that no zeros lie on the positive real w_1 axis. Figures 7.11a and b illustrate these results.

In a similar manner, we can represent the energy spectrum $\Phi_O(u)$ as an analytic function $o(z_1)o^*(z_2^*)$; the conjugate function to $o(w_1)$ is just $o(1/w_1)$ so that $\Phi_O(w_1)$ can be written as a polynomial of degree $2N$:

$$\Phi_O(w_1)=C^2\prod_{j=1}^{N}(w_1-w_{1,j})(w_1-1/w_{1,j}^*). \tag{7.79}$$

That is, the complex zeros of $\Phi_O(w_1)$ consist of the original N zeros of the object transform plus their inverses. This is illustrated in Fig. 7.11c.

Thus, the essence of the phase problem is that, without some basis for choosing between the correct zero and its inverse, we could construct $2^{N/2}$ equally valid sets of N zeros each representing a real, possibly positive, object. In the one-dimensional case, there is no unique solution to the phase problem, in either a theoretical or practical sense; additional information is required to find the object intensity.

Consider now the two-dimensional case, where the Fourier transform of the object intensity can be written as a polynomial in two complex variables,

$$o(w_1,w_2)=\sum_{n=0}^{N}\sum_{m=0}^{M}O_{nm}w_1^n w_2^m. \tag{7.77}$$

NAPIER and BATES [7.89] were the first to find that a unique solution to the phase problem was more likely to occur in this case. In one dimension, ambiguity resulted from the factorizability of the polynomial (7.77a); in two dimensions, as shown by BRUCK and SODIN [7.88], ambiguity may also exist if the two variable polynomial (7.77) is factorizable (or reducible) and the degree of ambiguity is determined by the number of non-self-conjugate irreducible factors. However, there is a very small probability that any two-dimensional polynomial is reducible; in fact, reducible polynomials in two dimensions are a set of measure zero [7.90]. Thus one is tempted to assume that the two-dimensional phase problem has a unique solution "almost always".

The uniqueness of the two-dimensional phase problem is the subject of much current research. The results of applying the algorithms to be described in Sect. 7.4.3 strongly suggest that effectively unique solutions may exist for certain objects, although of course it is always possible to produce counter-examples [7.91, 92]. FIDDY et al. [7.93] and FIENUP [7.94] have used Eisenstein's irreducibility theorem to define one particular class of objects for which a unique solution is guaranteed.

There are three basic approaches to solving the phase problem in stellar speckle interferometry. In the first, it is assumed that something about the object is known. For example, for a symmetric object intensity

$$O(\alpha,\beta)=O(-\alpha,-\beta), \tag{7.80}$$

the Fourier transform $o(u,v)$ is purely real and continuity arguments enable it to be found from $|o(u,v)|$; a rotationally symmetric object is included in this category. Speckle holography, to be discussed in the next subsection, also assumes that the object has a known property. In the second approach, one assumes that the two-dimensional phase problem is almost unique and seeks an algorithm to recover the object intensity from the modulus information alone. In the third approach, additional information is extracted from the speckle images in a number of different ways (Sects. 7.4.4–7).

7.4.2 Speckle Holography

The technique of speckle holography, in its original and most elementary form [7.95, 96], relies on the presence of a reference object, preferably a point source. Let the object field be written as the sum of a point centered at the origin and the object under investigation $O_1(\alpha,\beta)$ centered at (α_1,β_1),

$$O(\alpha,\beta)=\delta(\alpha)\delta(\beta)+O_1(\alpha-\alpha_1,\beta-\beta_1). \tag{7.81}$$

The spatial autocorrelation of (7.81) consists of four terms

$$\begin{aligned}C_O(\alpha,\beta)=&\int_{-\infty}^{\infty}\int\delta(\alpha')\delta(\beta')\delta(\alpha'+\alpha)\delta(\beta'+\beta)d\alpha'd\beta'\\&+\int_{\infty}^{\infty}\int O_1(\alpha',\beta')O_1(\alpha'+\alpha,\beta'+\beta)d\alpha'd\beta'\\&+O_1(\alpha-\alpha_1,\beta-\beta_1)+O_1(-\alpha-\alpha_1,-\beta-\beta_1).\end{aligned} \tag{7.82}$$

The first two terms are located in the region of the origin, the third is the object centered at (α_1,β_1) and the fourth term is a 180° rotation of the object centered at $(-\alpha_1,-\beta_1)$. Provided that $\alpha_1>3a/2$ and $\beta_1>3b/2$, where the object extent is (a,b), the third and fourth terms are separated in angle from the first two and a reconstruction of the object is obtained (with the 180° rotation ambiguity). WEIGELT [7.97–99] has demonstrated that this is a useful astronomical technique and Fig. 7.12 shows an

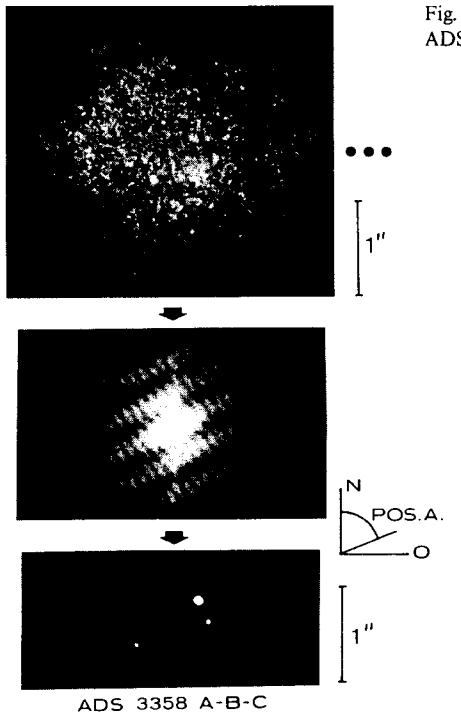

Fig. 7.12. Speckle holography of ADS 3358 [7.98]

example of the reconstruction of a triple star using speckle holography. The extent of the atmospheric isoplanatic angle is clearly important in speckle holography (Sect. 7.2.7).

If the reference point is not separated by the "holographic distance" then, in general, the object intensity cannot be reconstructed unambiguously unless further information is available. For example, LIU and LOHMANN [7.100] suggested using the long-exposure image as a mask, and BALDWIN and WARNER [7.101] used the knowledge that one star is brighter than the others to unravel the object (star clusters) from the autocorrelation function. Indeed, if the object consists of a discrete set of points and no vector separation between points occurs more than once (i.e., non-redundant spacings) then a unique solution to the problem exists [7.102, 103]. In another special case described by BRUCK and SODIN [7.87], a one-dimensional object can be reconstructed uniquely provided that the reference point is not in line with the object in the two-dimensional plane. The irreducibility criterion described by FIDDY et al. [7.93] also involves the use of reference points less than the usual holographic distance.

WEIGELT [7.104, 105] has suggested a technique called "speckle masking" that is related to holography in the sense that the speckle short-exposure images are preprocessed to yield an approximation to the instantaneous point spread function. In a more general sense, the speckle masking method involves the determination of the triple correlation

$$C_I(\alpha,\beta;\alpha_0,\beta_0)\equiv\langle I(\alpha,\beta)\cdot I(\alpha-\alpha_0,\beta-\beta_0)*I(\alpha,\beta)\rangle,$$

from which the triple correlation of the object,

$$C_O(\alpha,\beta;\alpha_0,\beta_0)\equiv[O(\alpha,\beta)\cdot O(\alpha-\alpha_0,\beta-\beta_0)]*O(\alpha,\beta),$$

can be determined by subtraction of bias terms [7.105]. Depending upon the complexity of the object, it is possible to determine $O(\alpha,\beta)$ from the triple correlation $C_O(\alpha,\beta;\alpha_0,\beta_0)$.

7.4.3 Modulus—Only Algorithms

In this approach to object reconstruction in stellar speckle interferometry, it is implicitly assumed that the two-dimensional problem *does* have a unique solution. Three algorithms that attempt to recover this solution are described below. Any result produced by these algorithms is therefore subject to two uncertainties: a) did a unique solution to the phase problem exist, even in principle? b) if it did exist, did the algorithm converge to this solution? Strictly speaking, uniqueness of the solution to the two-dimensional phase problem is not guaranteed and none of the algorithms described here have been shown to always converge to the unique solution when one is known, a priori, to exist. On the other hand, the overwhelming proportion of experimental evidence suggests that, for simple objects, some of these methods are successful in reconstructing object maps.

Iterative Algorithm

FIENUP has suggested a number of iterative algorithms [7.106–110] for computing the object intensity from a knowledge of only the modulus of its Fourier transform and an estimate of the support of the object. Two possible schemes are shown in Fig. 7.13. The first scheme, called the error reduction method because the mean square error between iterations always decreases [7.110], is a generalized form of the GERCHBERG-SAXTON algorithm [7.111]. Starting with an estimate of the object intensity at the k th iteration $\hat{O}_k(\alpha,\beta)$, the transform $\hat{o}_k(u,v)$ is calculated.

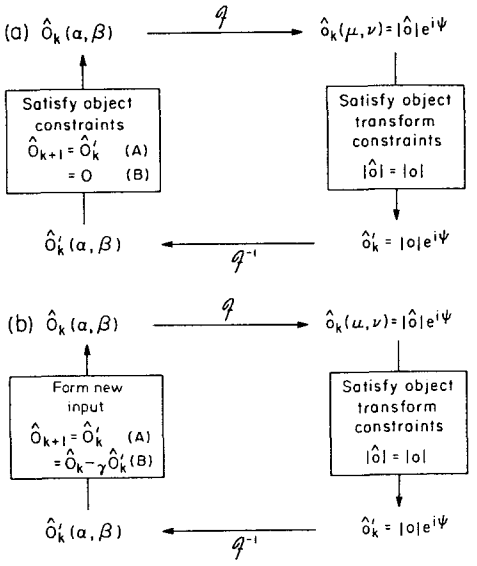

Fig. 7.13a, b. Two iterative algorithms for solving the phase problem. (a) error reduction—in object space, (A) is where object constraints are satisfied, (B) is where they are not satisfied; (b) hybrid input-output [7.110]

The modulus of this transform is replaced by the given modulus, forming a new estimate $\hat{o}'_k(u,v)$ that satisfies the constraints of the problem in the Fourier transform domain. This is inverse-transformed to give a new estimate of the object $\hat{O}'_k(\alpha,\beta)$ which is set to zero in the region where the object is known to be zero and set equal to zero where negative object values exist, thus forming a new estimate $\hat{O}_{k+1}(\alpha,\beta)$ which is the starting point for the next cycle. In practice, the error reduction algorithm converges very slowly and it is generally most useful when applied with one of the "input-output" algorithms.

The second scheme is shown in Fig. 7.13b and is called the "input-output" algorithm. The only difference between this and the error reduction scheme lies in how the next starting input $\hat{O}_{k+1}(\alpha,\beta)$ is derived from the previous output estimate $\hat{O}'_k(\alpha,\beta)$ and input $\hat{O}_k(\alpha,\beta)$. To a first-order approximation, a small change in the input gives a small change in the output proportional to that in the input (plus nonlinear terms); thus, by changing the input it should be possible to drive the output in the desired direction. The most satisfactory version of this scheme, called the hybrid input-output algorithm is

$$\begin{aligned}\hat{O}_{k+1}(\alpha,\beta) &= \hat{O}'_k(\alpha,\beta) \quad \text{when object constraints satisfied}\\ &= \hat{O}_k(\alpha,\beta)-\gamma\hat{O}'_k(\alpha,\beta) \quad \text{when not satisfied,}\end{aligned} \tag{7.83}$$

where γ is a parameter, typically on the order of unity.

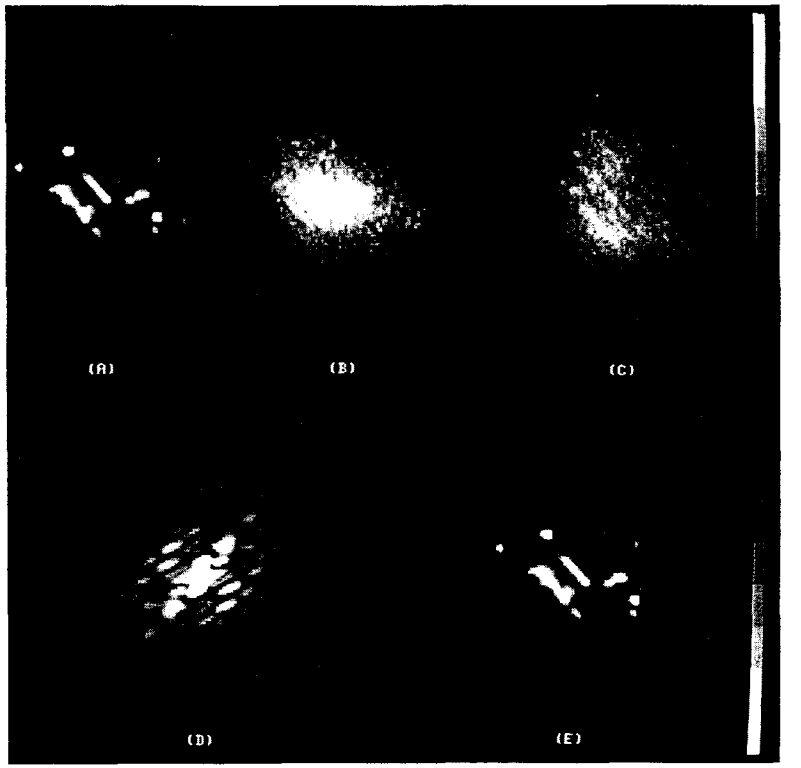

Fig. 7.14. (A) Original object; (B), (C) examples of simulated degraded images; (D) Fourier modulus estimate computed from degraded images; (E) image reconstructed using iterative algorithm [7.110]

A discussion of the relative merits of different iterative algorithms is given in [7.110]; at the present time, these algorithms are still rather ad hoc and their success appears to depend to some extent on the skill of the programmer. Figure 7.14 shows some results obtained by Fienup. These algorithms tends to successfully recover the object intensity for simple, but non-symmetric, objects; the shape of the support of the object also appears to affect the success of the iterative method. It should be stressed that this (and other) algorithms can fail to converge to the correct solution for complicated objects.

Phase-Closure Algorithms

BATES and coworkers [7.112–114] have suggested an algorithm that, in its original form, may be useful as a starting point for the Fienup

algorithm [7.115–117], and in a future improved form may be valuable on its own. Consider an array of N by M values of the Fourier transform of an object (for a real object of size N by N, $M=N/2+1$); the aim of this algorithm is to calculate the phases of each point θ_{ij}, allowing any one point (usually the origin) to be set to zero. Bates and coworkers suggested the following two step procedure:

i) Estimate the magnitude of the $(N-1)$ by M phase differences along the u-axis, $|\theta_{i+1,j}-\theta_{i,j}|$ and the N by $(M-1)$ v-phase differences $|\theta_{i,j+1}-\theta_{i,j}|$.

ii) Compute the N by M phases from the magnitudes of these $(2NM-N-M)\cong 2NM$ phase differences.

Let us assume, for the moment, that step (i) is possible and see how phase closure might be used to determine the phases. Consider the rectangle comprising the first four points (0,0), (1,0), (1,1), and (0,1) and assume that the magnitudes of the four phase differences are known:

$$\begin{aligned} |\theta_{1,0}-\theta_{0,0}| &= \psi_1, \\ |\theta_{1,1}-\theta_{1,0}| &= \psi_2, \\ |\theta_{1,1}-\theta_{0,1}| &= \psi_3, \\ |\theta_{0,1}-\theta_{0,0}| &= \psi_4. \end{aligned} \tag{7.84}$$

Clearly, we can set

$$\theta_{0,0}=0 \tag{7.85a}$$

and

$$\theta_{1,0}=+\psi_1. \tag{7.85b}$$

(If in fact $\theta_{1,0}=-\psi_1$, the object reconstruction will be rotated by 180°.) Proceeding around the rectangle anti-clockwise,

$$\theta_{1,1}=\psi_1\pm\psi_2 \tag{7.85c}$$

and this leads to four possible values of $\theta_{0,1}$,

$$\theta_{0,1}=\psi_1\pm\psi_2\pm\psi_3. \tag{7.85d}$$

On the other hand, going directly from (0,0) to (0,1) yields

$$\theta_{0,1}=\pm\psi_4 \tag{7.85e}$$

BATES [7.112] argued that only one of the four solutions (7.85d) will equal one of the two solutions (7.85e), thus determining the phases at each of the four points. If this is the case, then this procedure could be repeated for all points in the Fourier plane and the object intensity could be found by inverse Fourier transformation. Since the number of phase difference magnitudes is roughly twice the number of phases, it may be possible to use the methods mentioned in Sect. 7.4.7 for improving the phase estimates.

Even if the above step (ii) works, it is still necessary to find the magnitudes of phase differences, step (i). These can be estimated by oversampling the modulus in a scheme in which the Shannon interpolation formula is replaced by two point interpolation [7.112]; this provides only a crude estimate of the phase differences (for example, a large proportion have to be set equal to 0 or π) and requires improvement for reliable object restoration by itself. Combined with a modified Fienup algorithm that incorporates a preprocessing step to remove the strong central lobe in the Fourier plane, this technique has been shown [7.116, 117] to produce excellent reconstructions of simple objects.

Maximum Entropy Algorithm

In general terms, the maximum entropy method reconstructs the smoothest object intensity distribution consistent with the available data. It was first suggested for use with phaseless data by GULL and DANIELL [7.118]; as with the other algorithms, there is of course no way that the maximum entropy algorithm can resolve any inherent ambiguities [7.119]. If there are ambiguities, this method restores the smoothest object map.

7.4.4 Use of Exponential Filters

The ambiguity of the phase problem arises because the $2N$ zeros of the object energy spectrum consist of the N zeros associated with the Fourier transform of the object, plus their inverses. Given only the $2N$ zeros of the energy spectrum, it is impossible, in general, to select the correct zeros from each zero pair. By making a second measurement of the energy spectrum of a modified object intensity distribution [the original $O(\alpha,\beta)$ multiplied by $\exp(-2\pi\alpha a)$, where a is a constant], it is possible to unambiguously recover the correct N zeros and hence the object intensity itself. This was first suggested by WALKER [7.120] and WOOD et al. [7.121].

The basic principle of the method is shown in Fig. 7.15, where, for illustration, there are only three sets of zeros. The zeros corresponding to the original object are shown as solid circles ● and their inverses as ○; given only the object energy spectrum it is impossible to determine which

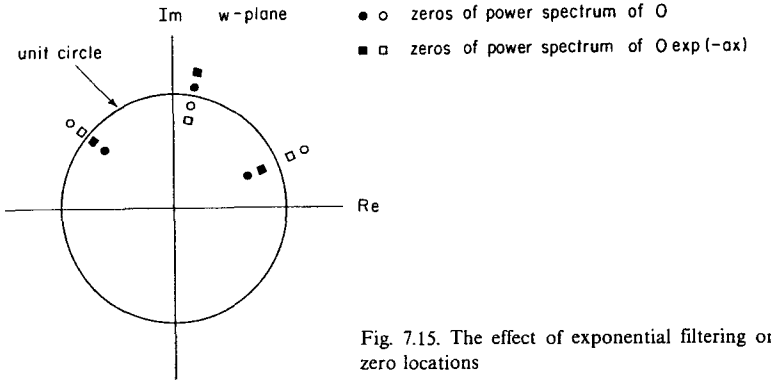

Fig. 7.15. The effect of exponential filtering on zero locations

is the "correct" one. When the object is multiplied by $\exp(-2\pi\alpha a)$, $a>0$, the zeros in terms of the z-variable move from z_j to $z_j - ia$, and in terms of the w-variable, $w=\exp(-2\pi i z\Delta)$, from w_j to $w_j\exp(2\pi a\Delta)$; that is, the correct zeros all move radially outwards by a constant factor, as shown in Fig. 7.15 (●→■). The energy spectrum of the modified object contains both these zeros (■) and their inverses (□); given both pairs of zeros (●, ○, ■ and □) the correct zero (●) can always be located. Although our description has been in terms of one dimension, the uniqueness of the solution also applies to the two-dimensional case.

In astronomy, it is, of course, impossible to place an exponential filter over the object! WALKER [7.122] showed that this is not necessary and that the exponential filter may be placed in the image plane. Denote the instantaneous image intensity by $I(\alpha,\beta)$ and the exponential filter transmittance by $G(\alpha,\beta)$. The energy spectra of the image intensity and the modified image intensity $(I(\alpha,\beta)\cdot G(\alpha,\beta))$ are

$$\Phi_I(u,v)=|o(u,v)|^2\,\langle|T(u,v)|^2\rangle \tag{7.5}$$

and

$$\begin{aligned}\Phi'_I(u,v)&=\langle|i(u,v)\circledast g(u,v)|^2\rangle\\&=\langle|\{o(u,v)T(u,v)\}\circledast g(u,v)|^2\rangle,\end{aligned} \tag{7.86}$$

where $\circledast$ denotes convolution and the other symbols are defined in Sect. 7.2.1.

Provided that

$$G(\alpha_1+\alpha_2,\beta_1+\beta_2)\equiv G(\alpha_1,\beta_1)G(\alpha_2,\beta_2), \tag{7.87}$$

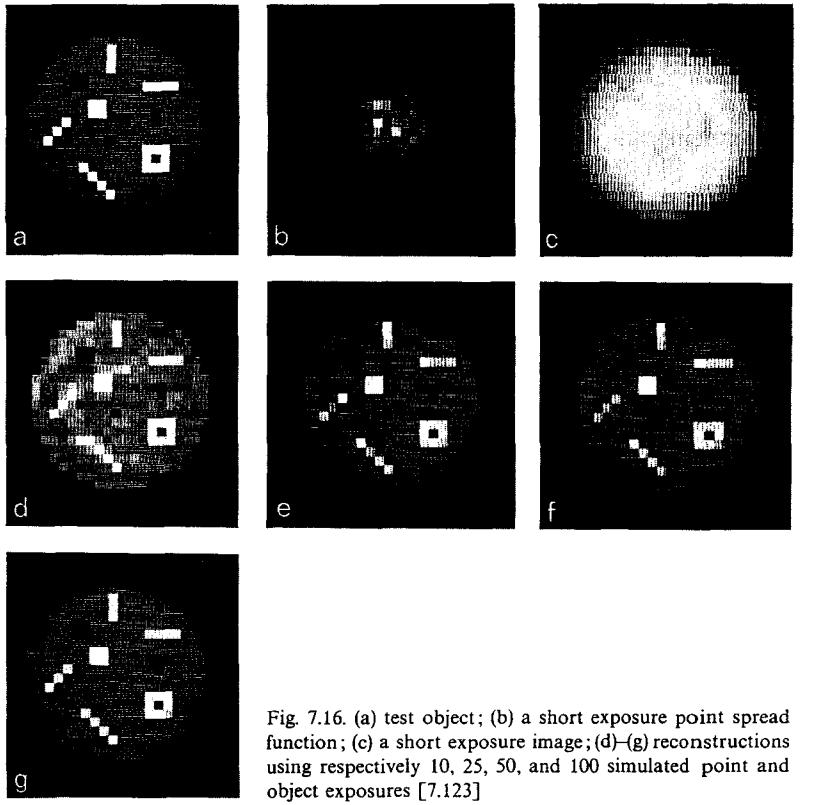

Fig. 7.16. (a) test object; (b) a short exposure point spread function; (c) a short exposure image; (d)–(g) reconstructions using respectively 10, 25, 50, and 100 simulated point and object exposures [7.123]

which is satisfied by the real exponential function, the convolution of (7.86) simplifies to yield

$$\Phi'_I(u,v)=|o'(u,v)|^2\,\langle|T'(u,v)|^2\rangle \tag{7.88}$$

where,

$$o'(u,v)=o(u,v)\circledast g(u,v)$$

and

$$T'(u,v)=T(u,v)\circledast g(u,v).$$

Assuming that the forms of the two transfer functions $\langle|T(u,v)|^2\rangle$ and $\langle|T'(u,v)|^2\rangle$ can be found (using a reference star, for example), we can find

the energy spectra of the object and of the modified object which are sufficient data for a unique solution to the phase problem.

Having shown that a unique object reconstruction can be found from $|o(u,v)|^2$ and $|o'(u,v)|^2$, there remains the problem of finding a practical two-dimensional algorithm that converges to this unique solution. WALKER [7.122, 123] has used an extended version of the Fienup algorithm that includes both sets of Fourier constraints. Figure 7.16 shows an example of reconstructions obtained by WALKER in a computer simulation, using this algorithm. It should be noted that this proposed method of object reconstruction uses only a single set of data for the object and for the reference, as the exponential filter can be applied numerically on the raw data.

7.4.5 Shift and Add

The short-exposure speckle images shown in Fig. 7.1 are of an unresolvable star in the upper row and α-Orionis, or Betelgeuse, which is a red giant star in the lower row. In simplistic terms, each "speckle" in both sets of images may be regarded as an "image"; for the upper row, it is an image of a point source and for the lower row it is an image of α-Orionis. Such reasoning led HARVEY and coworkers [7.124, 125] to obtain the first diffraction-limited map of a star other than our own sun.

In the original method, a few bright speckles are selected from each exposure and superimposed with the aid of a digital microdensitometer and computer. Figure 7.17 shows the result of this process for a point object (a) and α-Orionis in the continuum (b) and TiO absorption band (c); clearly the giant star is resolved and the difference |(b–c)| indicates possible temperature variation over the surface of the star. MCDONNELL and BATES [7.126] have applied superresolution techniques to produce an enhanced image of Betelgeuse from this data.

This approach to forming object maps has been extended by BATES and CADY [7.127, 128] in a technique they call "shift and add". Let (α_j, β_j) denote the coordinates of the center of the brightest speckle in the jth image; each image is shifted such that (α_j, β_j) is at the origin and then added to all other similarly shifted images, giving the result

$$R(\alpha,\beta)=\frac{1}{N}\sum_{j=1}^{N} I_j(\alpha-\alpha_j,\beta-\beta_j). \tag{7.89}$$

This process is carried out for both the object under study and a reference star; the image of the object is de-convolved using that of the reference and an algorithm such as "CLEAN" [7.129]. A theoretical study [7.130] has recently confirmed that diffraction-limited information is preserved in the shift and add method.

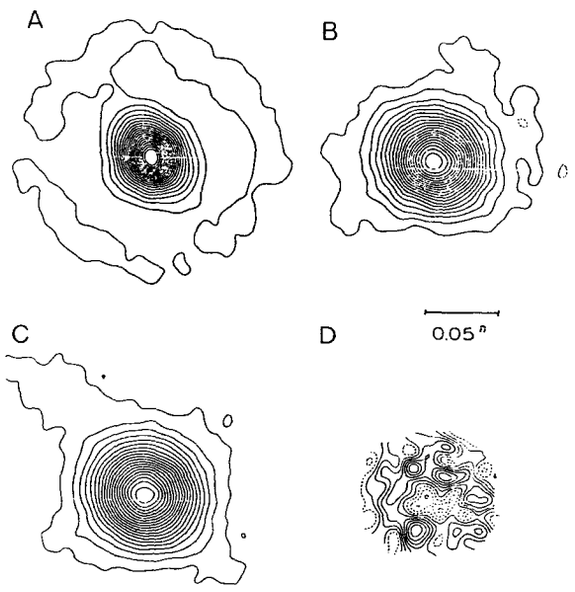

Fig. 7.17A–D. Diffraction-limited images computed from short exposure photographs by LYNDS et al. [7.124]. (A) unresolved star (γ-Ori), (B) α-Ori or Betelgeuse, in the continuum, (C) α-Ori in the TiO band and (D) the difference image (B)–(C). The contour levels are 5% of the peak intensity (A)–(C); in (D) the interval is 2%, with the broken curve indicating that the continuum is brighter

7.4.6 Phase Averaging

In the technique of speckle interferometry, the Fourier transforms of the instantaneous image intensity and the object intensity are related by

$$i(u,v)=o(u,v)T(u,v), \tag{7.90}$$

where $T(u,v)$ is the instantaneous transfer function. The quantities $\langle|i(u,v)|^2\rangle$ and $\langle|T(u,v)|^2\rangle$ are measured and an estimate of the object energy spectrum $|o(u,v)|^2$ is obtained. Taking the logarithm of (7.90) we obtain

$$\text{phase}\{i(u,v)\}=\text{phase}\{o(u,v)\}+\text{phase}\{T(u,v)\} \tag{7.91}$$

and, taking the average

$$\langle \text{phase}\{i(u,v)\}\rangle = \text{phase}\{o(u,v)\} + \langle \text{phase}\{T(u,v)\}\rangle , \tag{7.92}$$

where, in all cases, the phase is the value in the interval $-\infty$ to ∞. Thus, provided that $\langle \text{phase}\{T(u,v)\}\rangle$ is known (or zero), the phase of the object transform can be obtained from the average phase of the image transforms; this method was first suggested by MCGLAMERY [7.131].

Using arguments based on the central limit theorem, it is not difficult to show that, for $D \gg r_0$ and angular frequencies

$$r_0/\lambda < (u,v) < (D-r_0)/\lambda ,$$

the quantity $T(u,v)$ is a circular complex Gaussian random process; it follows that

$$\langle \text{phase}\{T(u,v)\}\rangle = 0 ,$$

and that the phase $\{T(u,v)\}$ folded into the primary interval $-\pi$ to π is statistically uniformly distributed.

The crucial step in implementing the phase-averaging method is therefore the determination of the "unwrapped" phase (i.e., that in the interval $-\infty$ to ∞) from the phase in the primary interval $-\pi$ to π. In principle, this may be done by assuming continuity of the phase and following it out from the origin where it can be assumed to be zero. This procedure is subject to error when the modulus $|i(u,v)|$ is small; O'DONNELL [7.36] has shown that the root-mean-square absolute error σ in the unwrapped phase is given approximately by

$$\sigma \simeq \frac{1}{(2\bar{N})^{1/2}|\hat{i}(u,v)|} , \tag{7.93}$$

where $\bar{N}$ is the average number of detected photons per frame and $\hat{i}(u,v)$ is the Fourier transform of the instantaneous image intensity normalized to unity at the origin. Clearly, a small value of $|\hat{i}(u,v)|$ leads to a large error. For example, for a point object $[\hat{\Phi}_O(u,v)=1]$ at an intermediate frequency $[T_D(u,v)\simeq 0.5]$ and a large telescope $(D/r_0 \simeq 40)$, an *average* value of $|\hat{i}(u,v)|$ is on the order of 10^{-2}, implying $\bar{N} > 8\times 10^4$ detected photons per frame for a phase error of less than 0.25 rad.

Despite the above analysis, computer simulations of the phase averaging method have shown some promise [7.132, 133], particularly for providing a starting point to the Fienup algorithm. Other algorithms for phase unwrapping have been suggested by TRIBOLET [7.134] and SWAN [7.135]; in the latter, the average phase is calculated without explicit unwrapping. Finally, MERTZ [7.74] has suggested following the phases of the angular frequency components in time in order to find their average value; the error has not yet been evaluated for this approach.

7.4.7 Knox-Thompson Method

In this method, first suggested by KNOX and THOMPSON [7.136, 137], the cross-energy spectrum of the image intensity is computed; following the notation of Sect. 7.2.1

$$\begin{aligned}&\langle i(u',v')i^*(u'',v'')\rangle \\ &\quad = o(u',v')o^*(u'',v'')\langle T(u',v')T^*(u'',v'')\rangle .\end{aligned} \tag{7.94}$$

Taking logarithms of each side and equating imaginary parts, we find that,

$$\begin{aligned}&\text{phase}\{\langle i(u,v)i^*(u+\Delta u, v+\Delta v)\rangle\} \\ &\quad = \text{phase}\{o(u,v)\} - \text{phase}\{o(u+\Delta u, v+\Delta v)\} \\ &\qquad + \text{phase}\{\langle T(u,v)T^*(u+\Delta u, v+\Delta v)\rangle\} ,\end{aligned} \tag{7.95}$$

where we have made the substitutions

$$\Delta u = u''-u' \quad \text{and} \quad \Delta v = v''-v' \quad \text{in (7.94).}$$

Thus, provided that

i) $\langle T(u,v)T^*(u+\Delta u, v+\Delta v)\rangle \neq 0$ and

ii) phase $\{\langle T(u,v)T^*(u+\Delta u, v+\Delta v)\rangle\}$ is either known or zero, it is possible to find *phase differences* in the object spectrum. This information is then used to find the phase of the object spectrum and hence the object intensity (if the energy spectrum is known). In the following we show that (i) is satisfied when $(u,v) < r_0/\lambda$ and that phase $\{\langle T(u,v)T^*(u+\Delta u, v+\Delta v)\rangle\}$ is approximately zero; we then discuss how the phase difference information can be used to restore the actual phases.

To evaluate the quantity $\langle T(u',v')T^*(u'',v'')\rangle$ we use a similar approach to that given in Sect. 7.2.3 to evaluate the approximate speckle transfer function. In particular, it is assumed that the complex amplitude of the wave in the telescope pupil from a point source is a circular complex Gaussian process. Instead of (7.23) we now have the following

expression for $\langle T(u',v')T^*(u'',v'')\rangle$:

$$\begin{aligned}
&\langle T(u',v')T^*(u'',v'')\rangle \\
&\quad = T_0(u',v')T_0^*(u'',v'')T_s(u',v')T_s^*(u'',v'') \\
&\qquad + \mathscr{S}^{-2}\int\int_{-\infty}^{\infty}\int\int T_s\left(\frac{\Delta\xi}{\lambda},\frac{\Delta\eta}{\lambda}\right)T_s^*\left(\frac{\Delta\xi}{\lambda}+\Delta u,\frac{\Delta\eta}{\lambda}+\Delta v\right) \\
&\qquad \cdot H_0(\xi_1,\eta_1)H_0^*(\xi_1+\lambda u',\eta_1+\lambda v')H_0^*(\xi_2,\eta_2) \\
&\qquad \cdot H_0(\xi_2+\lambda u'',\eta_2+\lambda v'')d\xi_1 d\eta_1 d\xi_2 d\eta_2 ,
\end{aligned} \tag{7.96}$$

where

$$\Delta\xi=\xi_1-\xi_2, \quad \Delta\eta=\eta_1-\eta_2,$$
$$\Delta u=u''-u', \quad \Delta v=v''-v',$$

and the other symbols were defined in Sect. 7.2.3. Assuming that $H_0(\xi,\eta)$ is constant where $T_s(\xi/\lambda,\eta/\lambda)$ is effectively non-zero, the second term reduces to, see (7.24),

$$\begin{aligned}
&\mathscr{S}^{-2}\int\int_{-\infty}^{\infty} T_s\left(\frac{\Delta\xi}{\lambda},\frac{\Delta\eta}{\lambda}\right)T_s^*\left(\frac{\Delta\xi}{\lambda}+\Delta u,\frac{\Delta\eta}{\lambda}+\Delta v\right)d\Delta\xi\, d\Delta\eta \\
&\cdot \int\int_{-\infty}^{\infty}|H_0(\xi,\eta)|^2\left|H_0\left(\xi+\lambda\left(\frac{u''+u'}{2}\right),\eta+\lambda\left(\frac{v''+v'}{2}\right)\right)\right|^2 d\xi\, d\eta .
\end{aligned} \tag{7.97}$$

Bearing in mind that the seeing transfer function $T_s(u,v)$ has a width $\simeq r_0/\lambda$, that it is clear from (7.97) that $\langle T(u,v)T^*(u+\Delta u,v+\Delta v)\rangle$ can only be non-zero if $|\Delta u|$ and $|\Delta v|<r_0/\lambda$ [otherwise the first integral in (7.97) is zero].

If we make the further approximation that the seeing transfer function has a Gaussian shape [it is more accurately described by (7.17)], then it is straightforward to show that

$$\begin{aligned}
&\langle T(u,v)T^*(u+\Delta u,v+\Delta v)\rangle \\
&\quad \simeq \langle|T(u,v)|^2\rangle\,|T_s(\Delta u/2,\Delta v/2)|^2 .
\end{aligned} \tag{7.98}$$

That is, the Knox-Thompson transfer function is simply the product of the speckle transfer function at (u,v) and the squared modulus of the seeing transfer function at $(\Delta u/2,\Delta v/2)$. It follows from (7.98) that

$$\text{phase}\,\langle T(u,v)T^*(u+\Delta u,v+\Delta v)\rangle \simeq 0 .$$

Since (7.98) results from an oversimplified atmospheric model, it cannot be relied upon quantitatively, but it does provide the correct qualitative condition on $|\Delta u|$ and $|\Delta v|$. Using the log-normal model, FRIED [7.48] suggests that the optimum value of $|\Delta u|$ and $|\Delta v|$ is approximately $0.2r_0/\lambda$.

If we consider the Fourier transform of the object to be sampled on a grid of N by M points there are approximately $2NM$ phase differences for a single choice of $(\Delta u,\Delta v)$; several schemes have been suggested for efficiently computing the required NM phases [7.138–145]. This problem is similar to that of calculating phases from shearing interferograms. It may be helpful to use more than one value of $(\Delta u,\Delta v)$ [7.140].

In a variation of the Knox-Thompson technique, AITKEN and DESAULNIERS [7.146] suggest computing average ratios $\langle i(u,v)/i(u+\Delta u,v+\Delta v)\rangle$, a possible advantage being that a separate reference calibration may not be required. SHERMAN [7.147] has extended the technique to non-isoplanatic imaging. BRAMES and DAINTY [7.148] have given an interpretation of the method in terms of the complex zero picture of Sect. 7.4.1; this picture may be useful for studying the role of noise in the technique. The effects of photon noise on speckle image reconstruction with the Knox-Thompson algorithm have recently been investigated [7.149]. Photon noise introduces a frequency-dependent bias which must be corrected for successful reconstruction. In the photon-limited case (low light levels), NISENSON and PAPALIOLIOS [7.149] gave the lower bound on the number of frames M required for "good" image reconstruction of a point-like object as

$$M \geqq 125\left(\frac{N_{sp}}{\bar{N}}\right)^2 ,$$

where N_{sp} is the average number of speckles per frame and $\bar{N}(<N_{sp})$ is the average number of detected photons per frame.

7.4.8 Summary

In this section we have reviewed a number of possible techniques for solving the phase problem, that is, reconstructing the object intensity, in stellar speckle interferometry. The methods fall into two categories; those that require only the modulus of the object Fourier transform (covered in Sects. 7.4.2 and 3) and those that utilize other information present in the original speckle exposures (Sects. 7.4.4 to 7). It seems obvious that methods in the latter category are preferable for this particular phase problem, since they make use of additional information present in the available data.

Although substantial progress in this topic has been made in the last few years, the map of Betelgeuse obtained by HARVEY and coworkers in 1975 remains the *only* non-trivial stellar object reconstructed from speckle data. The practical difficulties in implementing the algorithms on real astronomical data are frequently underestimated. Part of this difficulty arises because the implementation of ordinary speckle interferometry also has a number of practical problems that have to be overcome if photometric accuracy is desired; some of these practical problems are discussed in the following section.

7.5 Implementation

7.5.1 Data Collection and Processing

Speckle camera systems have been constructed by a number of groups [7.143, 150–154]. As an example, we shall describe a "first-generation" system used at Kitt Peak National Observatory for many years [7.153], a diagram of which is shown in Fig. 7.18.

Referring to Fig. 7.18, light from the telescope passes through an electromechanical shutter (1) at the front of the speckle camera system and reaches the Cassegrain or Richey-Chretien focus at (2). At the 4 m Mayall telescope, the image scale at this focus is approximately 6.5 arcsec/mm so that a lens (3) is required to magnify the image 10 or 20 times giving final image scales of approximately 0.65 and 0.32 arcsec/mm, respectively. At 500 nm, the diffraction-limited angular frequency of a 4 m telescope is approximately 40 arcsec^{-1}, and the sampling theorem therefore requires image plane sampling at $\Delta\alpha \leqq 0''.012$, or 0.04 mm or less in the 20× magnified image plane; this value also determines the resolution (or MTF) of the image detection system.

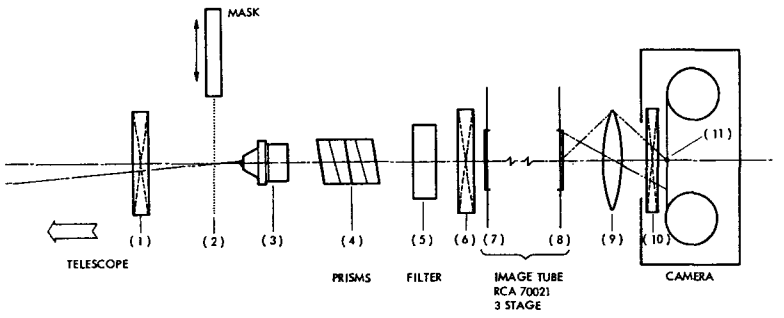

Fig. 7.18. Schematic cross-section view of a speckle camera [7.153]

It is necessary to correct for atmospheric dispersion except when observing close to the zenith. The magnitude of atmospheric dispersion depends upon a number of factors [7.155], but it is approximately given by

$$\Delta z \cong 0.3 \tan z \quad \text{arcsec/100 nm},$$

in the middle of the visible spectrum. Either a grating system [7.150, 152] or a pair of Risley prisms [7.151, 153] can be used to correct this; Fig. 7.18 shows the use of a prism pair. The optimum choice of glasses for the prisms are LaK24 and KF9 [7.156]—these match the dispersion of air over the broadest wavelength range. A narrow-band interference filter (5) selects the mean wavelength and bandpass (see Sect. 7.2.6 for a discussion of the permissable bandpass).

The most critical element in a speckle camera system is the image detector. Figure 7.18 shows an image intensifier/photographic film combination, which has the advantage of simplicity. A variety of image intensifiers may be suitable—magnetically or electrostatically focussed cascade systems, or microchannel plate devices; a variable (high) gain and low background are two practical requirements for the intensifier. Recently constructed speckle cameras and those under construction all use some form of electronic readout; this has the potential advantages of overcoming the noise and nonlinearity of photographic film and of allowing the possibility of real-time analysis of the data.

The type of electronic image detector required depends to a certain extent on the type of astronomical speckle observations that are planned and the intended method of data analysis. Before describing possible detectors it is therefore appropriate to discuss methods of data reduction. In the first-generation speckle cameras, the photographic images were analyzed in a coherent optical processor; this extremely simple analog device gives as output the energy spectrum of the complex amplitude transmittance of the film, the average energy spectrum being found by summation of the energy spectra of M frames ($M < 1000$ in practice). This technique could also be used for other "real-time" photographic-type detectors [7.139], but these analog systems tend to suffer from nonlinearities and noise. Digital processing appears to offer more flexibility and is the only way of implementing some of the object reconstruction algorithms described in Sect. 7.4.

For conventional speckle interferometry, there are two approaches to calculating the object information; one is via the average energy spectrum, as in (7.5), and the other is via the average spatial autocorrelation function as in (7.3). Allowing for moderate oversampling, large telescope speckle data requires a format of at least 256 × 256 pixels and a

Fig. 7.19. Output of a vector autocorrelator display in real time when observing a binary star (courtesy of B. L. Morgan and H. Vine, Imperial College, London)

desirable frame rate is approximately $50\,s^{-1}$. Devices that compute Fourier transforms of this size at this rate are becoming available, but their cost may not be justified in this application. Consequently, the average energy spectrum method of analysis is currently done after the observations have been made and stored on a suitable medium such as videotape.

On the other hand, the autocorrelation method of analysis lends itself to real-time computation. VOKAC [7.157] has described a prototype on-line digital autocorrelator for 16-level (4 bit) 64×64 pixel images taken at a rate of $2\,s^{-1}$, and predicted that full-scale throughout would be possible with current technology. BLAZIT [7.158] and the London group [7.159] have constructed one-bit vector autocorrelators that process images containing a few photons (<200) at $25\,s^{-1}$. Vector autocorrelators work on the principle that the autocorrelation function of an image consisting entirely of ones and zeros (presence or absence of a photon) is equal to the histogram of vector differences between all possible pairs of photons. This algorithm can either be hardwired in a special purpose device or programmed into a fast commercial or customized microcomputer. An example of the resolution of a binary star obtained with such a device (in real-time) is shown in Fig. 7.19. Another approach suggested by COLE [7.160] uses optical circuit elements to allow higher photon rates.

Depending upon the type of data analysis to be used, there are several possible electronic detector systems. One of the most straightforward is

to use an intensified television camera or intensifier plus television camera combination. The format of the data allows easy storage on videotape, but digital computer analysis, via a video-digitiser system, may be tedious. Another possibility is to replace the television camera by a charge-coupled device (CCD) [7.161]. The advantage of both of these approaches is that either analog (intensity) or digital (photon counting) data may be processed. For low light levels, photon counting devices in which the position and time of photoelectron events are recorded may be preferable [7.162, 163], particularly since the recorded data is already in a suitable format for vector autocorrelation processing.

It should also be noted that speckle interferometry can also be accomplished using a single or twin photomultipliers [7.164] or with a linear array [7.165], but there seems no advantage apart from cost and only bright objects can be studied. Equipment for laboratory simulation of stellar speckle interferometry has also been described [7.166].

7.5.2 One-Dimensional Infrared Speckle Interferometry

Efficient two-dimensional array detectors in the near infrared (2–5 μm) are not yet widely available and therefore infrared speckle interferometry has to be practised using only a single detector element. This feature, some other special problems that are encountered and its demonstrated astronomical success, make it worthwhile to devote a section of this review to infrared speckle interferometry.

At first glance, infrared speckle interferometry would seem less fruitful then that in the visible range, particularly in view of the restriction to a single detector element. Table 7.1 summarizes the resolution according to the diffraction-limit for a 4 m telescope (column 2) and the seeing limit (column 4) for the wavelengths of 0.5, 2.2(K), 3.45(L), and 4.8(M) μm. From column (2), it can be seen that the diffraction-limited angular resolution (Rayleigh criterion) is approximately 0".03 at 0.5 μm,

Table 7.1.

(1) Wavelength [μm]	(2) $\Delta\alpha$ ($D=4$ m) [arcsec]	(3) r_0 [m]	(4) ω [arcsec]
0.5	0.03	0.1	1.00
2.2 (K)	0.14	0.6	0.74
3.45 (L)	0.22	1.0	0.68
4.8 (M)	0.30	1.5	0.64

but only 0".30 at 4.8 μm, whereas a 1".0 seeing limited image at 0.5 μm is slightly smaller, 0".64, at 4.8 μm. Thus, taking the ratio of columns (2) and (4), we see that there is typically a 33 times increase in angular resolution possible by doing speckle interferometry at 0.5 μm, whereas the improvements at 2.2, 3.45, and 4.8 μm are only 5, 3 and 2, respectively (this does assume "good" seeing). The reason why infrared speckle has been so valuable is that, despite the relatively poorer angular resolution, there are many more potentially resolvable (i.e., large) bright objects in the near infrared than in the visible. Some infrared speckle observations are summarized in Sect. 7.6.5.

The technique of one dimensional infrared speckle interferometry is described in [7.167–171], particularly the comprehensive paper by SIBILLE et al. [7.168]. In the method developed by the French group, the image is scanned over a long, narrow slit and the light collected by a single indium antimonide (InSb) detector cooled to liquid nitrogen or helium temperature. The bandwidth restrictions are much less severe in the infrared than in the visible [see (7.37) and Table 7.1] the maximum $\Delta\lambda/\bar{\lambda}$ being on the order of 0.13 at 2.2 μm and 0.37 at 4.8 μm. The scanning speed of the image across the slit has to be sufficient to "freeze" the speckle, rates of 50–100 arcsec s^{-1} being typical; the effect of scanning rate is described by AIME et al. [7.172].

If the scan is assumed to be along the α-axis (corresponding to the u-axis in the angular frequency plane), the temporal average energy spectrum $\langle|i(f)|^2\rangle$ of the image intensity $I(t)\equiv I(\alpha/v)$, where v is the scan rate, is given by

$$\langle|i(f)|^2\rangle = |o(u,0)|^2\langle|T(u,0)|^2\rangle T_{\text{slit}}^2(u)\,, \tag{7.99}$$

where the temporal frequency f is related to the angular frequency u by $f=uv$ and where the slit transfer function for a slit of width α_{slit} is

$$T_{\text{slit}}(u)=\frac{\sin(\pi u\alpha_{\text{slit}})}{\pi u\alpha_{\text{slit}}}. \tag{7.100}$$

The one-dimensional temporal energy spectrum can easily be computed on-line using a commercial microcomputer. By observing a reference star, the speckle transfer function can be found, so that a section through the modulus of the object energy spectrum $|o(u,0)|$ can be found. The complete modulus could in principle be found by rotating the scan direction, although because of practical problems connected with atmospheric instability only north-south and east-west scans are usually made.

One of the greatest problems encountered in implementing infrared speckle interferometry is the instability of atmospheric turbulence.

Because the seeing limited angular frequency portion of the speckle transfer function is a significant part of the whole transfer function, it is not possible to use Worden's scheme for self-calibrating the method (Sect. 7.2.8). Accordingly, a typical observing sequence is object→sky→reference→sky→object, taking perhaps 100–1000 scans of each and repeating the sequence until consistent results are obtained. The "sky" measurement is required in the infrared due to emission from both the sky and the telescope, and an estimate of the energy spectrum of the object is obtained from

$$|o(u,0)|^2 \cong \frac{\langle|i_{\text{obj}}(f)|^2\rangle-\langle|i_{\text{sky}}(f)|^2\rangle}{\langle|i_{\text{ref}}(f)|^2\rangle-\langle|i_{\text{sky}}(f)|^2\rangle}. \tag{7.101}$$

The signal-to-noise ratio of the slit scan method is derived by SIBILLE et al. [7.168]. In addition to the atmospheric fluctuation and photon noise of the signal that are the only fundamental contributions in the visible, there is now also the photon noise of the "sky" background and noise inherent in the detector, such as Johnson noise. Limiting magnitudes, based on the value of the object intensity that yields an energy spectrum equal to that of the noise sources for a single 100 ms scan, were predicted to be of the order of 5 to 6 for the K, L, and M wavelengths, although practical experience indicates limiting magnitudes of approximately 7 (K) to 2 (M). SELBY et al. [7.167] used a grating rather than a slit, thus measuring only a single-frequency component at a time; they claim fainter limiting magnitudes but these have not yet been achieved.

In a new development of one-dimensional speckle interferometry (visible or infrared) AIME et al. [7.173] suggested the use of a telescope with a one-dimensional aperture (e.g. $10\times800\,\text{cm}^2$). This gives a contrast gain over a circular aperture and, associated with a spectroscope, allows investigation of the spectral-angular plane with no loss in light.

7.6 Astronomical Results

Observational speckle interferometry is now over a decade old, and approximately 80 papers primarily concerned with astronomical results have been published, some of which are referenced below. Despite the enthusiasm of a few astronomers, it is only realistic to point out that the technique is not widely used or accepted by the astronomical community at large. Some possible reasons for this are: (i) relatively few objects, particularly in the visible, are resolvable by 4 m class telescopes, whose diffraction-limit at 400 nm are 0".02; (ii) calibration problems make it

difficult to obtain photometric energy spectra of sufficient accuracy for the particular astronomical problem; and (iii) only the most expensive equipment yields faint limiting magnitudes and enables the vast amounts of data to be reduced.

The summary of astronomical results given below is divided into four parts; solar system objects, binary stars, single stars and infrared objects. In addition to these, some more unusual objects have also been observed using speckle interferometry. For example, HEGE et al. [7.73] resolved one of the components of the "triple" quasar PG 1115+08 as a binary, one of the faintest objects studied by the speckle method ($m_v \simeq 16.2$). The Seyfert galaxy NGC 1068 has been observed in the visible [7.159] and at 2.2 μm [7.174], both results revealing a nuclear core containing most of the luminosity.

7.6.1 Solar System Objects

The angular diameters of the asteroids Pallas and Vesta were measured by WORDEN et al. [7.54, 175, 176], the results for Pallas indicating some elongation of the object. The diameter of the planetary satellites Rhea and Iapetus [7.176] and Titan [7.177] have also been measured.

Observations of the planet Pluto and its moon Charon are near to the limiting magnitude of speckle interferometry, their magnitudes being approximately 15.3 and 16.9, respectively. ARNOLD et al. [7.178] estimate Pluto's diameter to be 3000 ± 400 to 3600 ± 400 km depending upon whether limb darkening is incorporated in the model. This is slightly smaller than that measured by BONNEAU and FOY [7.179], 4000 ± 400 km with no limb darkening, who also estimate the diameter of Charon to be 2000 ± 200 km and propose a revised orbit for the moon. Both results imply a mean density of Pluto (and Charon) $\simeq 0.5\ \mathrm{g\,cm^{-3}}$.

The Solar granulation has also been measured by speckle interferometry [7.180–182]; the main technical problem here is the absence of any reference source for estimation of the speckle transfer function. Image reconstruction techniques (using the Knox-Thompson algorithm) have been applied to solar features [7.182].

7.6.2 Binary Stars

Speckle interferometry has been most successful when used to determine the angular separation and position angle of binary stars. MCALISTER [7.183–188] has reported over 1000 measurements of resolved binaries, and 500 binary stars unresolved by the speckle method [7.189, 190], as well as a number of detailed studies of individual systems [7.191–198].

Several hundred observations have also been reported by three other groups [7.7, 45, 199–206]. Several reasons have contributed to the success of speckle interferometry in this area; the measurements are amongst the simplest speckle observations to make, can be made rapidly on brighter stars (MCALISTER [7.207] reported 125 to 175 observations per clear night) and yield an accuracy far exceeding visual observations. MCALISTER [7.207] mentioned typical errors of 0.6% on the separation and $\pm 2°$ on the position angle, although other groups gave more conservative error estimates [7.201].

In principle, the fringe visibility can be used to estimate the magnitude difference of the two components of a binary star, but this requires proper calibration of the system using a reference star. MORGAN et al. [7.199] have built doubly-refracting prisms and a polarizer to enable artifical double-stars of known magnitude difference to be recorded for calibration purposes. It is typical of the gap between the theory and practice of speckle interferometry that the measurement of Δm, which is so simple in theory is, in practice, elusive.

The aim of making binary star measurements is usually to estimate the masses of each component. For a double-lined spectroscopic binary (i.e., one for which the radial velocities of both components are known) a minimum of two measurements of the angular separation and position angle yields both the masses of each component and the absolute distance (parallax). One example measured by MCALISTER [7.193] is 12 Persei; the masses are 1.25 ± 0.20 and 1.08 ± 0.17 times the mass of the Sun and parallax is $0''.046 \pm 0''.002$ which combined with the known apparent magnitudes gives absolute visual magnitudes of 3.8 ± 0.1 and 4.1 ± 0.1, respectively.

Binaries that are both double-lined spectroscopic and resolvable by speckle interferometry are rather rare. If the binary is single-lined, then speckle observations cannot unambiguously give the individual masses and distances. However, if masses appropriate to the spectral type are assumed, a distance can be found. MCALISTER [7.192] and MORGAN et al. [7.201] have applied this to binaries in the Hyades cluster, a distance marker in the universe, to confirm that its mass-luminosity relationship is normal and that its distance is approximately 10% greater than the original proper motion studies indicated.

BECKERS [7.208, 209] has suggested a modification of the speckle technique called "differential speckle interferometry" that may enable sub-milliarcsecond separation of binary stars to be measured on a 4 m class telescope in the visible. The technique uses the Doppler shift and observation at two closely spaced wavelengths to modulate the position of speckles in the short-exposure photographs; since the speckle procedure measures shifts to an accuracy of a fraction of the speckle size,

resolution of binaries whose separation is much less than the diffraction-limit may be possible.

7.6.3 Single Resolvable Stars

One of the first stellar discs to be resolved by speckle interferometry was the supergiant α-Orionis (Betelgeuse) [7.7] which has subsequently been observed on several occasions [7.124, 125, 203, 210–212], including the first example of a map of a star apart from our Sun [7.124]. Whilst there is evidence for substantial limb darkening on α-Orionis, the speckle energy spectrum provides rather low quality data for comparison with models. Measurements reported by Goldberg et al. [7.212] at H_α wavelength and the neighboring continuum reveal a mean diameter of 0".060 with an unresolvable bright feature near the SW limb in the continuum and significant H_α emission at large distances (radii exceeding 0".25). The diameter of the giant star α-Bootis has also been estimated [7.213].

Several Mira variable stars—*o*-Ceti (Mira), R. Leo and χ Cygni [7.210, 214, 215]—have been observed by speckle interferometry. These results indicate that Mira-type stars probably have smaller diameters than was previously supposed.

Finally we note that the first results of long-baseline two telescope speckle interferometry have resolved the individual components of the binary star Capella, yielding values of 5 ± 1 and $4 \pm 2 \times 10^{-3}$ arcsec [7.216].

7.6.4 Infrared Stars

Although infrared speckle interferometry is at the moment still restricted to a single detector across which the image is scanned, many interesting measurements have been made. This work is likely to expand when array infrared detectors become available.

The diameters of several protostar candidates have been measured, particularly WS–IRS 5, MonR 2–IRS 3, S 140–IRS 1 and the BN object [7.169, 171, 217–219]. MCCARTHY's measurements of the triple nature of MonR 2–IRS 3 [7.219] are a good example of the results possible with careful data analysis. The bright carbon star IRC+10216 has been observed both the continuum and in the CO lines [7.220, 221]. Several Mira variables [7.171, 220] and the dust shells around Wolf-Rayet stars [7.222] and the supergiant α-Orionis [7.169] have also been observed. The star T-Tauri, after which the class of T-Tauri variable stars is named, has been shown to be double [7.223]. Finally, object restoration via the Knox-Thompson algorithm and image enhancement techniques have been applied to the extended object η-Carinae [7.224].

Acknowledgements. This review was written whilst the author was on leave from the University of Rochester at the School of Electrical Engineering, The University of Sydney as the recipient of a Norman I. Price Scholarship. It is a pleasure to acknowledge the hospitality of Professor T. W. Cole, Dr. J. Davis, and Dr. W. H. Steel in Sydney and also the financial support of the U.S. Air Force under Grant AFOSR-81-0003. I wish to thank Evelyn Snyder for her expert typing of the manuscript.

References

7.1 Fizeau: Compt. Rend. **66**, 932 (1868)
7.2 M. Born, E. Wolf: *Principles of Optics*, 6th ed. (Pergamon, London 1980) p. 508
7.3 A. A. Michelson: Nature **45**, 160 (1891)
7.4 A. A. Michelson, F. G. Pease: Astrophys. J. **53**, 249 (1921)
7.5 R. Hanbury Brown: *The Intensity Interferometer* (Taylor and Francis, London 1974)
7.6 A. Labeyrie: Astron. Astrophys. **6**, 85 (1970)
7.7 D. Y. Gezari, A. Labeyrie, R. V. Stachnik: Astrophys. J. **173**, L 1 (1972)
7.8 J. C. Dainty: Symposium on Recent Advances in Observational Astronomy, ed. by H. L. Johnson and C. Allen (Ensenada, Mexico 1981) p. 95. A bibliography on stellar interferometry is maintained by the author and is available on request
7.9 C. Roddier, F. Roddier: In *Image Formation from Coherence Functions in Astronomy*, ed. by C. van Schooneveld (Reidel, Dordrecht 1979) p. 175
7.10 J. Davis: NZ J. Science **22**, 451 (1979)
7.11 R. H. T. Bates: Phys. Rep. **90**, 203 (1982)
7.12 J. C. Dainty (ed.): *Laser Speckle and Related Phenomena*, Topics Appl. Phys., Vol. 9 (Springer, Berlin, Heidelberg, New York 1975) Chap. 7
7.13 A. Labeyrie: *Progress in Optics* **14**, 47 (North-Holland, Amsterdam 1976)
7.14 S. P. Worden: Vistas in Astron. **20**, 301 (1977)
7.15 A. Labeyrie: Ann. Rev. Astron. Astrophys. **16**, 77 (1978)
7.16 High Angular Resolution Stellar Interferometry, Proceedings IAU Colloquium No. 50 (University of Sydney 1979)
7.17 Applications of Speckle Phenomena, Proc. SPIE **243** (SPIE, 1980)
7.18 A. Papoulis: *Probability, Random Variables and Stochastic Processes* (McGraw-Hill, New York 1965) p. 338 and 447
7.19 J. W. Goodman: *An Introduction to Fourier Optics* (McGraw-Hill, New York 1968), Chap. 6
7.20 J. W. Goodman: [Ref. 7.19, Eq. (6–26)], note that the form used in (7.11) assumes that $H(\xi, \eta)$ is the pupil function, and not its mirror image
7.21 R. E. Hufnagel, N. R. Stanley: J. Opt. Soc. Am. **54**, 52 (1964)
7.22 D. L. Fried: J. Opt. Soc. Am. **56**, 1372 (1966)
7.23 F. Roddier: Scientific Importance of High Angular Resolution at Infrared and Optical Wavelengths. Proc. ESO Conf. (March 1981) p. 5
7.24 F. Roddier: *Progress in Optics* **19**, 281 (North-Holland, Amsterdam 1980)
7.25 R. L. Fante: Proc. IEEE **63**, 1669 (1975) and **68**, 1424 (1980)
7.26 J. C. Dainty, R. J. Scaddan: Mon. Not. R. Astr. Soc. **170**, 519 (1975)

7.27 C. Roddier: J. Opt. Soc. Am. **66**, 478 (1976)
7.28 D. S. Brown, R. J. Scaddan: Observatory **99**, 125 (1979)
7.29 D. Korff: J. Opt. Soc. Am. **63**, 971 (1973)
7.30 J. C. Dainty: Opt. Commun. **7**, 129 (1973)
7.31 C. Aime, S. Kadiri, G. Ricort, C. Roddier, J. Vernin: Opt. Acta **26**, 575 (1979)
7.32 A. Chelli, P. Lena, C. Roddier, F. Sibille: Opt. Acta **26**, 583 (1979)
7.33 J. C. Dainty: Mon. Not. R. Astr. Soc. **169**, 631 (1974)
7.34 F. Roddier, G. Ricort, C. Roddier: Opt. Commun. **24**, 281 (1978)
7.35 D. P. Karo, A. M. Schneiderman: J. Opt. Soc. Am. **67**, 1277 (1977)
7.36 K. A. O'Donnell: Thesis, University of Rochester (1983)
7.37 A. W. Lohmann, G. P. Weigelt: Optik **53**, 167 (1979)
7.38 J. C. Dainty, D. R. Hennings, K.A. O'Donnell: J. Opt. Soc. Am. **71**, 490 (1981)
7.39 K. A. O'Donnell, B. J. Brames, J. C. Dainty: Opt. Commun. **41**, 79 (1982)
7.40 R. J. Scaddan, J. G. Walker: Appl. Opt. **17**, 3779 (1978)
7.41 G. Parry, J. G. Walker, R. J. Scaddan: Opt. Acta **26**, 563 (1979)
7.42 C. Roddier, F. Roddier: J. Opt. Soc. Am. **65**, 664 (1975)
7.43 F. Roddier, J. M. Gilli, G. Lund: J. Opt. **13**, 263 (1982)
7.44 D. P. Karo, A. M. Schneiderman: J. Opt. Soc. Am. **68**, 480 (1978)
7.45 B. L. Morgan, D. R. Beddoes, R. J. Scaddan, J. C. Dainty: Mon. Not. R. Astr. Soc. **183**, 701 (1978)
7.46 G. M. Morris: Appl. Opt. **20**, 2017 (1981)
C. G. Wynne: Opt. Commun. **28**, 21 (1979)
7.47 D. Korff, G. Dryden, R. P. Leavitt: J. Opt. Soc. Am. **65**, 1321 (1975)
7.48 J. H. Shapiro: J. Opt. Soc. Am. **66**, 469 (1976)
J. H. Shapiro: In *Laser Beam Propagation in the Atmosphere*, ed. by J. W. Strohbehn, Topics Appl. Phys., Vol. 25 (Springer, Berlin, Heidelberg, New York 1978) Chap. 3
7.49 D. L. Fried: Op. Acta **26**, 597 (1979)
7.50 F. Roddier, J. M. Gilli, J. Vernin: J. Opt. **13**, 63 (1982)
7.51 P. Nisenson, R. V. Stachnik: J. Opt. Soc. Am. **68**, 169 (1978)
7.52 A. M. Schneiderman, D. P. Karo: J. Opt. Soc. Am. **68**, 338 (1978)
7.53 G. P. Weigelt: Opt. Acta **26**, 1351 (1979)
7.54 S. P. Worden, M. K. Stein, G. D. Schmidt, J. R. P. Angel: Icarus **32**, 450 (1977)
G. L. Welter, S. P. Worden: J. Opt. Soc. Am. **68**, 1271 (1978)
7.55 Yu. M. Bruck, L. G. Sodin: Astron. Astrophys. **87**, 188 (1980)
7.56 S. P. Worden: SPIE Proc. **243**, 66 (1980)
7.57 J. G. Walker: Opt. Acta **28**, 885 (1981)
7.58 R. L. Fante: J. Opt. Soc. Am. **69**, 1394 (1979)
7.59 R. J. Keyes (ed.): *Optical and Infrared Detectors*, 2nd ed., Topics Appl. Phys., Vol. 19 (Springer, Berlin, Heidelberg, New York 1980)
7.60 M. E. Barnett, G. Parry: Opt. Commun. **21**, 60 (1977)
7.61 J. C. Dainty: Mon. Not. R. Astr. Soc. **183**, 223 (1978)
7.62 J. G. Walker: High Angular Resolution Stellar Interferometry, Proc. IAU Colloquium No. 50 (Univ. Sydney 1979)
7.63 J. G. Walker: Opt. Commun. **29**, 273 (1979)
7.64 A. H. Greenaway, J. C. Dainty: Opt. Commun. **35**, 307 (1980)
7.65 F. Roddier: Imaging in Astronomy, AAS/SAO/OSA/SPIE Topical Meeting, Reprints ThC6 (Boston 1975)
7.66 J. W. Goodman, J. F. Belsher: Proc. SPIE **75**, 141 (1976)
7.67 J. W. Goodman, J. F. Belsher: RADC-TR-76-50 (March 1976), RADC-TR-76-382 (December 1976), RADC-TR-77-175 (May 1977). All ARPA Order No. 2646 (Rome Air Development Center, Griffin AFB, NY 13441)
7.68 M. G. Miller: J. Opt. Soc. Am. **67**, 1176 (1977)

7.69 J. C. Dainty, A. H. Greenaway: J. Opt. Soc. Am. **69**, 786 (1979)
7.70 J. C. Dainty, A. H. Greenaway: High Angular Resolution Stellar Interferometry, Proc. IAU Colloquium No. 50 (Univ. Sydney 1979)
7.71 K. A. O'Donnell, J. C. Dainty: J. Opt. Soc. Am. **70**, 1354 (1980)
7.72 A. D. Code: *Astronomical Techniques* (University of Chicago Press, Chicago, IL1962) pp. 50–87
7.73 E. K. Hege, E. N. Hubbard, P. A. Strittmatter, S. P. Worden: Astrophys. J. **248**, L 1 (1981)
7.74 L. N. Mertz: Appl. Opt. **18**, 611 (1979)
7.75 H. A. Ferwerda: In *Inverse Source Problems*, ed. by H. P. Baltes, Topics Curr. Phys., Vol. 9 (Springer, Berlin, Heidelberg, New York 1978) Chap. 2
7.76 L. S. Taylor: IEEE Trans AP-**29**, 386 (1981)
7.77 A. H. Greenaway: J. Optics (Paris) **10**, 308 (1979)
7.78 Lord Rayleigh: Phil. Mag. **34**, 407 (1892)
7.79 E. Wolf: Proc. Phys. Soc. **80**, 1269 (1962)
7.80 K. Itoh, Y. Ohtsuka: Appl. Opt. **20**, 4239 (1981)
7.81 A. H. Greenaway: Opt. Commun. **42**, 157 (1982)
7.82 A. M. J. Huiser: Opt. Commun. **42**, 226 (1982)
7.83 R. H. T. Bates: Mon. Not. R. Astr. Soc. **142**, 413 (1969)
7.84 R. H. T. Bates, P. J. Napier: Mon. Not. R. Astr. Soc. **158**, 405 (1972)
7.85 R. E. Burge, M. A. Fiddy, A. H. Greenaway, G. Ross: Proc. R. Soc. Lond. Ser. A **350**, 191 (1976)
7.86 G. Ross, M. A. Fiddy, M. Nieto-Vesperinas, M. Wheeler: Proc. R. Soc. Lond. Ser. A **360**, 25 (1976)
7.87 M. A. Fiddy, G. Ross: Opt. Acta **26**, 1139 (1979)
7.88 Yu. M. Bruck, L. G. Sodin: Opt. Commun. **30**, 304 (1979)
7.89 P. J. Napier, R. H. T. Bates: Astron. Astrophys. Suppl. **15**, 427 (1974)
7.90 M. H. Hayes, J. H. McClellan: Proc. IEEE **70**, 197 (1982)
7.91 A. M. J. Huiser, P. van Toorn: Opt. Lett. **5**, 499 (1980)
7.92 P. van Toorn, A. H. Greenaway, A. M. J. Huiser: Preprint
7.93 M. A. Fiddy, B. J. Brames, J. C. Dainty: Opt. Lett. **8**, 96 (1983).
7.94 J. Fienup: J. Opt. Soc. Am. **73**, 1421 (1983)
7.95 R. H. T. Bates, P. T. Gough, P. J. Napier: Astron. Astrophys. **22**, 319 (1973)
7.96 P. T. Gough, R. H. T. Bates: Opt. Acta **21**, 243 (1974)
7.97 G. P. Weigelt: Optik **43**, 111 (1975)
7.98 G. P. Weigelt: Appl. Opt. **17**, 2660 (1978)
7.99 G. P. Weigelt: Proc. SPIE **243**, 103 (1980)
7.100 C. Y. C. Liu, A. W. Lohmann: Opt. Commun. **8**, 372 (1973)
7.101 J. E. Baldwin, P. J. Warner: Mon. Not. R. Astr. Soc. **182**, 411 (1978)
7.102 J. Christou: Opt. Commun. **37**, 331 (1981)
7.103 J. R. Fienup, T. R. Crimmins, W. Holsztynski: J. Opt. Soc. Am. **72**, 610 (1982)
7.104 G. P. Weigelt: Opt. Commun. **21**, 55 (1977)
7.105 G. Weigelt, B. Wirnitzer: Opt. Lett **8**, 389 (1983)
7.106 J. R. Fienup: Opt. Lett. **3**, 27 (1978)
7.107 J. R. Fienup: Opt. Engrg. **18**, 529 (1979)
7.108 J. R. Fienup: *Transformations in Optical Signal Processing* (SPIE, Bellingham, Washington 1982)
7.109 J. R. Fienup: RADC-TR-81-63 (May 1981) (Rome Air Development Center, Griffiss AFB, NY 13441)
7.110 J. R. Fienup: Appl. Opt. **21**, 2758 (1982)
7.111 R. W. Gerchberg, W. O. Saxton: Optik **35**, 237 (1972)
7.112 R. H. T. Bates: Optik **61**, 247 (1982)

7.113 K. L. Garden, R.H.T. Bates: Optik **62**, 131 (1982)
7.114 W. R. Fright, R. H. T. Bates: Optik **62**, 219 (1982)
7.115 R. H. T. Bates, W. R. Fright: J. Opt. Soc. Am. **73**, 358 (1983)
7.116 R. H. T. Bates: Comp. Graph. & Image Proc. (in press)
7.117 R. H. T. Bates, W. R. Fright: *Advances in Computer Vision and Image Processing*, Vol. 1, ed. by T. S. Huang (JAI Press, 1983) Chap. 5
7.118 S. F. Gull, G. J. Daniell: Nature **272**, 686 (1978)
7.119 J. C. Dainty, M. A. Fiddy, A. H. Greenaway: In *Image Formation from Coherence Functions in Astronomy*, ed. by C. van Schooneveld (Reidel, Dordrecht 1979) p. 95
7.120 J. G. Walker: Opt. Acta **28**, 735 (1981)
7.121 J. W. Wood et al.: Opt. Lett., **8**, 54 (1981)
7.122 J. G. Walker: Opt. Acta **28**, 1017 (1981)
7.123 J. G. Walker: Appl. Opt. **21**, 3132 (1982)
7.124 C. R. Lynds, S. P. Worden, J. W. Harvey: Astrophys. J. **207**, 174 (1976)
7.125 S. P. Worden, C. R. Lynds, J. W. Harvey: J. Opt. Soc. Am. **66**, 1243 (1976)
7.126 M. J. McDonnell, R. H. T. Bates: Astrophys. J. **208**, 443 (1976)
7.127 R. H. T. Bates, F. M. Cady: Opt. Commun. **32**, 365 (1980)
7.128 F. M. Cady, R. H. T. Bates: Opt. Lett. **5**, 438 (1980)
7.129 J. A. Hogbom: Astron. Astrophys. Suppl. **15**, 417 (1974)
7.130 B. R. Hunt, W. R. Fright, R. H. T. Bates: J. Opt. Soc. Am. **73**, 456 (1983)
7.131 B. L. McGlamery: NASA TR SP-256, 167 (1971)
7.132 W. J. Cocke: Steward Obs. Reprint No. **264** (1980)
7.133 B. T. O'Conner, T. S. Huang: Comp. Graph. Image Proc. **15**, 25 (1981)
7.134 J. M. Tribolet: IEEE Trans. ASSP **25**, 170 (1977)
7.135 H. W. Swan: Ph.D. Thesis, Stanford University (1982)
7.136 K. T. Knox, B. J. Thompson: Astrophys. J. **193**, L45 (1974)
7.137 K. T. Knox: J. Opt. Soc. Am. **66**, 1236 (1976)
7.138 P. Nisenson, D. C. Ehn: Proc. SPIE **75**, 83 (1976)
7.139 M. P. Rimmer: Appl. Opt. **13**, 623 (1974)
7.140 J. W. Sherman: Proc. SPIE **74**, 249 (1976)
7.141 R. L. Frost, C. K. Rushforth, B. S. Baxter: Appl. Opt. **18**, 2056 (1979)
7.142 B. R. Hunt: J. Opt. Soc. Am. **69**, 393 (1969)
7.143 P. Nisenson, R. Stachnik, C. Papaliolios, P. Horowitz: Proc. SPIE **243**, 88 (1980)
7.144 R. Stachnik, P. Niesenson, C. Papaliolios: *Solar Instrumentation – What's Next?* (Sunspot, New Mexico 1980)
7.145 P. Nisenson, R. Stachnik, C. Papaliolios: In *Optical and Infrared Telescopes for the 1990s*, ed. by A. Hewitt (Kitt Peak National Observatory, Tucson, AZ 1980) p. 401
7.146 G. J. M. Aitken, D. L. Desaulniers: Opt. Commun. **28**, 26 (1979)
7.147 J. W. Sherman: Proc. SPIE **243**, 51 (1980)
7.148 B. J. Brames, J. C. Dainty: J. Opt. Soc. Am. **71**, 1542 (1981)
7.149 P. Nisenson, C. Papaliolios: Opt. Commun. **45**, 311 (1983)
7.150 A. Labeyrie: Auxiliary Instrumentation for Large Telescopes (ESO/CERN, 1972) p. 389
7.151 D. R. Beddoes, J. C. Dainty, B. L. Morgan, R. J. Scaddan: J. Opt. Soc. Am. **66**, 1247 (1976)
7.152 A. M. Scheiderman, D. P. Karo: Opt. Engrg. **16**, 72 (1977)
7.153 J. B. Breckinridge, H. A. McAlister, W. G. Robinson: Appl. Opt. **18**, 1034 (1979)
7.154 G. Hubbard, K. Hege, M. A. Read, P. A. Strittmatter, N. J. Woolf, S. P. Worden: Astron. J. **84**, 1437 (1979)
7.155 G. W. Simon: Astron. J. **71**, 190 (1966)
7.156 E. P. Wallner, W. B. Wetherell: J. Opt. Soc. Am. **69**, 1413 (1979) (abstract only)
7.157 P. R. Vokac: Proc. SPIE **119**, 223 (1977)

7.158 A. Blazit: *Image Processing Techniques in Astronomy* (Reidel, Dordrecht 1975)
7.159 J. Meaburn, B. L. Morgan, H. Vine, A. Pedlor, R. Spencer: Nature **296**, 331 (1982)
7.160 T. W. Cole: Proc. ASA **4**, 19 (1980)
7.161 D. F. Barbe (ed.): *Charge-Coupled Devices*, Topics Appl. Phys., Vol. 38 (Springer, Berlin, Heidelberg, New York 1980)
7.162 C. Papaliolios, L. Mertz: Proc. SPIE **331**, 360 (1982)
7.163 L. N. Mertz, T. D. Tarbell, A. Title: Appl. Opt. **21**, 628 (1982)
7.164 A. A. Tokovinin: Sov. Astron. Lett. **4**, 204 (1978)
7.165 G. D. Schmidt, J. R. P. Angel, R. Harms: Publ. Astr. Soc. Pac. **89**, 410 (1977)
7.166 A. M. Schneiderman, P. F. Kellen, M. G. Miller: J. Opt. Soc. Am. **65**, 1287 (1975) D. P. Karo, A. M. Schneiderman: Appl. Opt. **18**, 828 (1979)
7.167 M. J. Selby, R. Wade, C. S. Magro: Mon. Not. R. Astr. Soc. **187**, 553 (1979)
7.168 F. Sibille, A. Chelli, P. Lena: Astron. Astrophys. **79**, 315 (1979)
7.169 R. R. Howell, D. W. McCarthy, F. J. Low: Astrophys. J. **251**, L21 (1981)
7.170 C. Perrier: ESO Messenger **29**, 26 (1981)
7.171 J. M. Mariotti, A. Chelli, R. Foy, P. Lena, F. Sibille, G. Tchountonov: Astron. Astrophys. **120**, 237 (1983)
7.172 C. Aime, S. Kadiri, G. Ricort: Opt. Commun. **35**, 169 (1980)
7.173 C. Aime, J. Demarcq, F. Martin, G. Ricort: Opt. Engrg. **22**, 224 (1983)
7.174 D. W. McCarthy, F. J. Low, S. G. Kleinmann, F. C. Gillett: Astrophys. J. **257**, L7 (1982)
7.175 S. P. Worden, M. K. Stein: Astron. J. **84**, 140 (1979)
7.176 S. P. Worden: *Asteroids* (Univ. Arizona Press 1979) p. 119
7.177 P. Nisenson, J. Apt, R. Goody, P. Horowitz: Astron. J. **86**, 1690 (1981)
7.178 S. J. Arnold, A. Boksenburg, W. L. W. Sargent: Astrophys. J. **234**, L159 (1979)
7.179 D. Bonneau, R. Foy: Astron. Astrophys. **92**, L1 (1980) (*See also* G. Baier, N. Hetterich, G. Weigelt: ESO Messenger **30**, 23 (1982))
7.180 J. W. Harvey, J. B. Breckinridge: Astrophys. J. **182**, L137 (1973)
7.181 J. W. Harvey, M. Schwarzschild: Astrophys. J. **196**, 221 (1975)
7.182 R. V. Stachnik, P. Nisenson, D. C. Ehn, R. H. Hudgin, V. E. Shirf: Nature **266**, 149 (1977)
7.183 H. A. McAlister: Astrophys. J. **215**, 159 (1977)
7.184 H. A. McAlister: Astrophys. J. **225**, 932 (1978)
7.185 H. A. McAlister, K. A. DeGioia: Astrophys. J. **228**, 493 (1979)
7.186 H. A. McAlister: Astrophys. J. **230**, 497 (1979)
7.187 H. A. McAlister, F. C. Fekel: Astrophys. J. Suppl. Ser. **43**, 327 (1980)
7.188 H. A. McAlister, E. M. Hendry: Astrophys. J. Suppl. Ser. **48**, 273 (1982)
7.189 H. A. McAlister: Publ. Astron. Soc. Pac. **90**, 288 (1978)
7.190 H. A. McAlister, E. M. Hendry: Publ. Astron. Soc. Pac. **93**, 221 (1981)
7.191 H. A. McAlister: Publ. Astron. Soc. Pac. **88**, 957 (1976)
7.192 H. A. McAlister: Astrophys. J. **212**, 459 (1977)
7.193 H. A. McAlister: Astrophys. J. **223**, 526 (1978)
7.194 H. A. McAlister: Astrophys. J. **236**, 522 (1980)
7.195 H. A. McAlister: Astron. J. **85**, 1265 (1980)
7.196 H. A. McAlister: Astron. J. **86**, 795 (1981)
7.197 H. A. McAlister: Astron. J. **86**, 1397 (1981)
7.198 H. A. McAlister, W. I. Hartkopf: Publ. Astr. Soc. Pac. **94**, 832 (1982)
7.199 B. L. Morgan, D. R. Beddoes, R. J. Scaddan, J. C. Dainty: Mon. Not. R. Astr. Soc. **183**, 701 (1978)
7.200 B. L. Morgan, G. K. Beckmann, R. J. Scaddan: Mon. Not. R. Astr. Soc. **192**, 143 (1980)

7.201 B. L. Morgan, G. K. Beckmann, R. J. Scaddan, H. A. Vine: Mon. Not. R. Astr. Soc. **198**, 817 (1982)
7.202 A. Labeyrie, D. Bonneau, R. V. Stachnik, D. Y. Gezari: Astrophys. J. **194**, L 147 (1974)
7.203 A. Blazit, D. Bonneau, L. Koechlin, A. Labeyrie: Astrophys. J. **214**, L 79 (1977)
7.204 D. Bonneau, A. Blazit, R. Foy, A. Labeyrie: Astron. Astrophys. Suppl. Ser. **42**, 185 (1980)
7.205 D. Bonneau, R. Foy: Astron. Astrophys. **86**, 295 (1980)
7.206 G. Weigelt: Astron. Astrophys. **68**, L 5 (1978)
7.207 H. A. McAlister: Modern Astrometry (IAU Colloquium No. 48, University Observatory Vienna 1978) p. 325
7.208 J. M. Beckers: Current Techniques in Double and Multiple Star Research (IAU Colloquium No. 62, Flagstaff, 1981)
7.209 J. M. Beckers: Opt. Acta **29**, 361 (1982)
7.210 D. Bonneau, A. Labeyrie: Astrophys. J. **181**, L 1 (1973)
7.211 M. S. Wilkerson, S. P. Worden: Astron. J. **82**, 642 (1977)
7.212 L. Goldberg, E. K. Hege, E. N. Hubbard, P. A. Strittmatter, W. J. Cocke: preprint C. Roddier, F. Roddier: Astrophys. J. **270**, L23 (1983)
7.213 S. P. Worden: Publ. Astr. Soc. Pac. **88**, 69 (1976)
7.214 A. Labeyrie, L. Koechlin, D. Bonneau, A. Blazit, R. Foy: Astrophys. J. **218**, L 75 (1977)
7.215 J. Christou, S. P. Worden: Astron. J. **85**, 302 (1980)
7.216 A. Blazit, D. Bonneau, M. Josse, L. Koechlin, A. Labeyrie, J. L. Onéto: Astrophys. J. **217**, L 55 (1977)
7.217 A. Chelli, P. Lena, F. Sibille: Nature **278**, 143 (1979)
7.218 H. M. Dyck, R. R. Howell: Astron. J. **87**, 400 (1982)
7.219 D. W. McCarthy: Astrophys. J. **257**, L 93 (1982)
7.220 R. Foy, A. Chelli, F. Sibille, P. Lena: Astron. Astrophys. **79**, L 5 (1979)
7.221 H. M. Dyck, S. Beckwith, B. Zuckerman: In press
7.222 D. A. Allen, J. R. Barton, P. T. Wallace: Mon. Not. R. Astr. Soc. **196**, 797 (1981)
7.223 H. M. Dyck, T. Simon, B. Zuckerman: Astrophys. J. **255**, L103 (1982)
7.224 A. Chelli, C. Perrier, Y. G. Biraud: Astron. Astrophys. **117**, 199 (1983)

Reprint from

Topics in Applied Physics

Volume 9: **Laser Speckle and Related Phenomena**
Editor: J. C. Dainty
Second Enlarged Edition

© by Springer-Verlag Berlin Heidelberg 1975 and 1984
Printed in Germany. Not for Sale.

Springer-Verlag
Berlin Heidelberg New York Tokyo